



Seismic response analysis of face slabs in concrete face rockfill dams

Miad Saberi, Charles-Darwin Annan & Jean Marie Konrad

To cite this article: Miad Saberi, Charles-Darwin Annan & Jean Marie Konrad (2019): Seismic response analysis of face slabs in concrete face rockfill dams, *Journal of Earthquake Engineering*, DOI: [10.1080/13632469.2019.1666756](https://doi.org/10.1080/13632469.2019.1666756)

To link to this article: <https://doi.org/10.1080/13632469.2019.1666756>



Published online: 28 Oct 2019.



Submit your article to this journal



Article views: 82



View related articles



View Crossmark data



Seismic response analysis of face slabs in concrete face rockfill dams

Miad Saberi^{a,b}, Charles-Darwin Annan^a, and Jean Marie Konrad^a

^aDepartment of Civil and Water Engineering, Université Laval, Québec, Canada; ^bGHD Limited, Montréal, Canada

ABSTRACT

The seismic behavior of the concrete slab in concrete-faced rockfill dams (CFRD) is investigated, considering concrete slab-cushion layer interface effect. The interface is simulated by an advanced constitutive model capable of simulating the complex behavior of soil–structure interfaces such as particle breakage, stress-dilatancy, stress-hardening, cyclic accumulative contraction, and stress degradation. Stage construction and reservoir impoundment of the dam are simulated and the dam is subjected to two earthquake records. The concrete slab responses under static and dynamic conditions are examined, and the effects of reservoir water level, interface roughness, and the interface modeling approach on the concrete slab response are investigated.

ARTICLE HISTORY

Received 4 October 2018
Accepted 9 September 2019

KEYWORDS

Concrete-faced rockfill dam;
soil–structure interface;
concrete face slab; static
response analysis;
earthquake ground motion
analysis; interface roughness

1. Introduction

Concrete-faced rockfill dams (CFRD) have been constructed increasingly over the past three decades. This is due to its low-cost and simple and rapid construction process (Cruz, Materón, and Freitas 2010; Gazetas and Dakoulas 1992; Sherard and Barry Cooke 1987; Uddin and Gazetas 1995). CFRDs, in general, consist of five essential components, including four zones (i.e. cushion, transition, main rockfill and secondary rockfill zones) and a concrete face slab laid on the upstream of the dam as illustrated in Fig. 1. Failure or damage to this impervious section of the dam would result in water penetration into the rockfill body and consequently weaken the dam stability (Dakoulas 2012a; Khalid et al. 1990; Saberi, Annan, and Konrad 2013; Uddin 1999; Zhou et al. 2016b). Earthquake ground motion is an important phenomenon that has caused severe damage to concrete face slabs in CFR dams. A typical example is the Zipingpu CFR dam which experienced severe concrete face failure under the May 12, 2008, Wenchuan magnitude 8.0 earthquake (Chen and Han 2009; Xianjing et al. 2011; Xu, Zou, and Liu 2012).

Numerical methods have been used to understand the behavior and performance of CFRDs under seismic events (Uddin and Gazetas 1995; Bayraktar, Dumanoglu, and Calayir 1996; Bayraktar, Hacifendioglu, and Muvafik 2005; Bayraktar, Kartal, and Adanur 2011; Uddin 1999; Kong and Liu 2002; Bayraktar and Kartal 2010; Kartal, Bayraktar, and Bas 2010; Seiphoori, Haeri, and Karimi 2011; Xianjing et al. 2011; Dakoulas 2012a, 2012b; Zou et al. 2013; Xu et al. 2015; Esfahani Kan and Taiebat 2016). Key among the critical behavior parameters is the behavior of the interface region between the concrete face slab and the

CONTACT Miad Saberi  miad.saberi.1@ulaval.ca;  miad.sabery@gmail.com  Department of Civil and Water Engineering, Université Laval, Québec, Canada; GHD Limited, Montréal, Canada

Color versions of one or more of the figures in the article can be found online at www.tandfonline.com/ueqe.

© 2019 Taylor & Francis Group, LLC

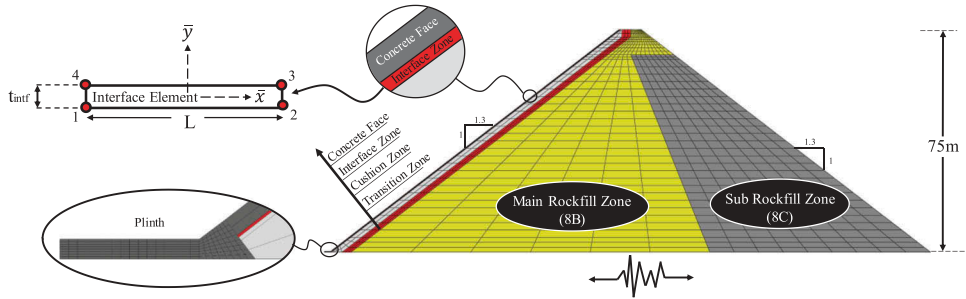


Figure 1. Typical cross-section of the case dam.

cushion layer made of gravel or rockfill. The interface plays an important role because of the interaction between the two main dam bodies having significantly different stiffnesses. The concrete slab-cushion layer interaction has been simulated widely by the contact analysis with Coulomb's friction law (Uddin and Gazetas 1995; Kong and Liu 2002; Zhang, Wang, and Shi 2004; Kartal, Bayraktar, and Bas 2010; Kartal, Bayraktar, and Basaga 2012; Seiphoori, Haeri, and Karimi 2011; Dakoulas 2012a, 2012b; Zhou et al. 2016b, 2016b; Modares and Quiroz 2016; Wen et al. 2017) and by zero-thickness elements with no volume change (Bayraktar, Kartal, and Adanur 2011; Justo, Segovia, and Jaramillo 1995; Khalid et al. 1990; Xianjing et al. 2011; Xu et al. 2015; Xu, Zou, and Liu 2012; Zou et al. 2013). Experimental observations (e.g. DeJong and Westgate 2009; DeJong, White, and Randolph 2006; Fakharian 1996; Hu and Pu 2004; Mortara, Mangiola, and Ghionna 2007; Uesugi, Kishida, and Uchikawa 1990; Zhang and Zhang 2006), however, indicate that the granular soil-structure interface has a thickness of about (5–10) D_{50} of adjacent granular soil (where D_{50} is the mean effective diameter) and therefore exhibits a different behavior from its adjacent materials. There is also evidence of a complicated volumetric behavior (i.e. phase transformation from contraction to dilation under shearing, accumulative contraction under cyclic loading and particle breakage) and stress-displacement relationships (i.e. stress hardening/softening, stress degradation, and stress path dependency) under different loading conditions. The interface may experience particle breakage under shear cycles, even at low to medium normal stresses (Zhang and Zhang 2006, 2009a). This phenomenon significantly increases the accumulative contraction behavior at the interface zones. Other experimental studies (e.g. DeJong and Westgate 2009; Fakharian 1996; Hu and Pu 2004; Shahrou and Rezaie 1997; Uesugi, Kishida, and Tsubakihara 1989) have also revealed that the structural surface roughness is an important element affecting the volumetric and stress-displacement behaviors in granular soil-structure interface systems. Furthermore, these interfaces can reach the critical state under large shear deformation; this behavior can be captured using the concept of critical state soil mechanics (CSSM) (DeJong and Westgate 2009; DeJong, White, and Randolph 2006; Fakharian 1996; Saberi, Annan, and Konrad 2018a).

The essential behaviors of granular soil-structure interfaces outlined above (i.e. phase transformation, accumulative contraction, particle breakage effect, critical state, stress hardening and degradation) cannot be addressed effectively using contact analysis or zero-thickness element with no volume change. The thin-layer interface element proposed by Zienkiewicz et al. (1970) and Desai, Lightner, and Siriwardane (1984) would be a preferred choice due to its capability to simulate volumetric behavior. Researchers have in the past

used the thin-layer interface elements for numerical studies of CFRDs with simple constitutive models such as the linear elastic model (Bayraktar and Kartal 2010), Clough and Duncan (1971) nonlinear elastic model (Chen et al. 2011), and the elastic-perfectly plastic model (Arici 2011). The thin-layer element type, however, needs to be used with an advanced interface constitutive model if it is to address the complex behaviors of granular soil–structure interface systems identified above. There are studies published in the literature in which the thin-layer element was used with advanced constitutive models for investigating the behavior of face slabs in CFRDs. For instance, Saberi, Annan, and Konrad (2018b, 2019) using the interface model developed in Saberi et al. (2016) studied the behavior of face slab under static conditions. Zhang and Zhang (2009b) using the interface model developed by Zhang and Zhang (2008), Xu et al. (2017), Qu et al. (2017), and Qu et al. (2019) using the interface model proposed by Liu, Zou, and Kong (2014) investigated the performance of face slabs in CFRDs under earthquake loading. Kong, Liu, and Zou (2016) also using the interface model by Liu, Zou, and Kong (2014) studied the separation process between the face slab and the cushion layer in CFR dams. However, there is still a need to investigate the effects of interface roughness and reservoir water level on the seismic behavior of concrete face slab in CFRDs by considering particle breakage at the concrete face-cushion interface zone.

This paper presents a two-dimensional seismic response analysis of the face slab in CFRDs using the finite element method (FEM). The main goal of this study is to investigate the effect of the interaction between the concrete slab and the cushion layer on the seismic response of the concrete face slab. The concrete face slab-cushion layer interaction is simulated explicitly using an advanced interface constitutive model recently developed by the authors (Saberi, Annan, and Konrad 2017). The interface model is capable of simulating the complex behavior of granular soil–structure interfaces under monotonic and cyclic loading, such as phase transformation, critical state, accumulative contraction, stress hardening, stress degradation, stress path dependency and particle breakage under shear cycles. The constitutive model is implemented into a finite element code in the form of a thin-layer interface element, and used in the seismic response analysis of the selected concrete-faced rockfill dam. The predicted responses of the CFR dam are compared with field observations, and the effect of face slab-cushion layer interaction on the response of the concrete face slab are examined under static and seismic load conditions, considering the effects of interface particle breakage and interface roughness. The effect of reservoir water level on the seismic response of the face slab is also investigated in this study. Responses are reported in terms of compressive and tensile stresses recorded in the concrete face slab, and results are compared with those of the simplified contact analysis approach.

2. The Selected Typical CFR Dam

A typical concrete-faced rockfill dam was selected and numerically simulated in this study. The geometry of the selected dam is similar to the Toulnustouc CFR dam, located 120 km north of the city of Baie-Comeau on the Toulnustouc River, in the North-East of Quebec, Canada. The dam is 75 m high and 575 m long and it is built on a bedrock foundation. The Toulnustouc dam has an embankment volume of about 1 452 000 m³ and a powerhouse with an installed capacity of 526 MW. The thickness of the concrete slab on the upstream face is 0.3 m. The dam has a crest width of about 7 m and the side slopes of 1.3 H: 1V down to the

foundation level (Bouzaiène, Chartrand, and Hammamji 2006; Hydro-Québec 2006). As the aspect ratio (crest length/height) of the selected dam is high (i.e. 575m/75m = 7.66), a two-dimensional plane-strain model and analysis provides sufficient accuracy (Arici 2011; Esfahani Kan and Taiebat 2016). Moreover, this analysis type is deemed sufficient for the purpose of simulating the effect of the face slab-cushion layer interaction on the response of the concrete face slab under earthquake ground motions. The cross-section of the dam is shown in Fig. 1. The material properties used to represent the selected dam were derived from the large-scale triaxial test data for typical large rockfill materials (Marachi, Chan, and Bolton 1972; Marsal 1967) as no triaxial test data exists on the Toulnustouc dam rockfill material.

3. Material Model

3.1. Rockfill

The Drucker–Prager constitutive model (Drucker, Gibson, and Henkel 1957) has been used widely for simulating granular materials, such as rockfill, in dam analysis (e.g. Bayraktar and Kartal 2010; Bayraktar, Kartal, and Adanur 2011; Kartal, Bayraktar, and Bas 2010; Kartal, Bayraktar, and Basaga 2012). The modified Drucker–Prager or Cap plasticity model originally proposed by DiMaggio and Sandler (1971) and Sandler and Baron (1979) has also been widely used for numerical modeling of granular soils (e.g. Helwany 2007; Khoei, Azami, and Haeri 2004; Loupasakis et al. 2009; Pichler et al. 2006; Saberi, Behnamfar, and Vafaeian 2015). In the present study, the cap plasticity model is used to simulate the rockfill zones of the case dam. The cap plasticity model employed considers the effect of stress history, stress path, dilatancy, and intermediate principal stress. The yield surface of the model has three segments: Drucker–Prager shear failure surface (F_s), an elliptical cap (F_c) surface and a transition surface (F_t) between the shear failure surface and the cap, as illustrated in Fig. 2a. The cap plasticity model simulates the elastic behavior using a linear elastic formulation once when the stress state is within the yield surface. The elastoplastic behavior is simulated once the stress state is on the yield surface. The formulation of Drucker–Prager failure surface, cap yield surface and transition surface are shown in Eqs. 1, 2 and 3, respectively.

$$F_s = t - p \tan \beta - d = 0 \quad (1)$$

$$F_c = \sqrt{(p - p_a)^2 + \left(\frac{Rt}{1 + \alpha_c - \alpha_c / \cos \beta} \right)^2} - R(d + p_a \tan \beta) = 0 \quad (2)$$

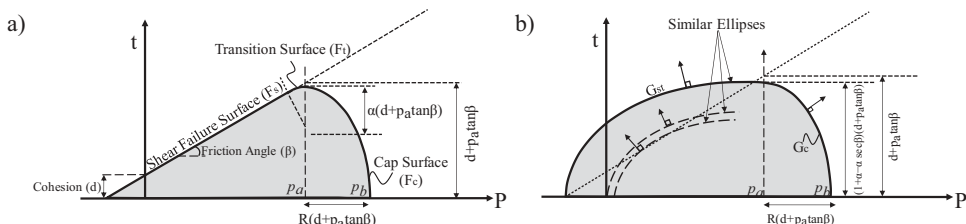


Figure 2. Cap plasticity surfaces in p - t plane, a) Yield surfaces and b) Flow potential.

$$F_t = \sqrt{(p - p_a)^2 + \left[t - \left(1 - \frac{\alpha_c}{\cos\beta} \right) (d + p_a \tan\beta) \right]^2} - \alpha_c (d + p_a \tan\beta) = 0 \quad (3)$$

Where $p = (\sigma_1 + \sigma_2 + \sigma_3)/3$ is mean effective stress, d and β are cohesion and soil friction angle in the p - t plane as illustrated in Fig. 2a. In Eq. 1, t is a measure of deviatoric stress and is calculated as $t = q/g$, in which q is deviatoric stress and g is a function controlling the shape of yield surface in the deviatoric plane (Π -Plane) defined by Eq. 4.

$$g = \frac{2K}{1 + K + (1 - K) \left(\frac{r}{q} \right)^3} \quad (4)$$

where K is a model parameter and r is the third invariant of deviatoric stress.

In Eq. 2, R is a model parameter controlling the shape of the cap and α_c is a small number defined for a smooth transition surface between the Drucker–Prager and the cap failure surfaces. p_a is an evolution term for controlling the hardening–softening behavior, and it is a function of the volumetric plastic strain.

The flow potential surface of the cap plasticity model in p - t plane is shown in Fig. 2b. The model assumes a non-associated flow rule for the Drucker–Prager and transition failure surfaces and an associated flow rule for the cap region. The potential surfaces corresponding to the Drucker–Prager failure and transition part (G_{st}) and the cap region (G_c) are given by Eqs. 5 and 6 respectively.

$$G_{st} = \sqrt{[(p_a - p) \tan\beta]^2 + \left(\frac{t}{1 + \alpha_c - \alpha_c/\cos\beta} \right)^2} \quad (5)$$

$$G_c = \sqrt{[(p - p_a)]^2 + \left(\frac{Rt}{1 + \alpha_c - \alpha_c/\cos\beta} \right)^2} \quad (6)$$

Further details about the model formulation can be found in Helwany (2007).

3.2. Interface

A thin-layer element defined by an advanced interface constitutive model proposed by Saberi, Annan, and Konrad (2017) is used for modeling the complex behavior of the concrete slab-cushion layer interface. The model is based on a two-dimensional (2D) plane-strain problem and a dry condition assumption. The thickness (t_{intf}) of the interface zone is assumed to be 5–10 times the mean effective diameter (D_{50}) of adjacent soil particles.

Stress and strain vectors in the interface model consist of normal and tangential components. Based on the basic theory of plasticity (Chen and Baladi 1985; Dafalias 1986), the relationship between increments of total stress vector ($d\sigma$) and increments of total strain vector ($d\epsilon$) can be expressed as

$$d\sigma = [D]^{ep} d\epsilon = \left[[D]^e - \frac{[D]^e R n^T [D]^e}{K_p + (n^T [D]^e R)} \right] d\epsilon \quad (7)$$

where $[\mathbf{D}]^{ep}$ is the elastoplastic stiffness matrix, $[\mathbf{D}]^e$ is elastic stiffness matrix, \mathbf{n} is the loading direction vector, \mathbf{R} is the flow direction vector and K_p is the plastic modulus. The superscript e represents the elastic component.

The elasticity matrix $[\mathbf{D}]^e$ links the stress increment and elastic strain increment vectors as (Lashkari 2013):

$$\begin{aligned} \left\{ \begin{array}{c} d\sigma_n \\ d\tau \end{array} \right\} &= [\mathbf{D}]^e \left\{ \begin{array}{c} d\varepsilon_n \\ d\varepsilon_t \end{array} \right\}^e = \begin{bmatrix} D_n & 0 \\ 0 & D_t \end{bmatrix} \left\{ \begin{array}{c} d\varepsilon_n \\ d\varepsilon_t \end{array} \right\}^e \\ &= \begin{bmatrix} D_{n0}\sqrt{\sigma_n/p_{atm}} & 0 \\ 0 & D_{t0}\sqrt{\sigma_n/p_{atm}} \end{bmatrix} \left\{ \begin{array}{c} d\varepsilon_n \\ d\varepsilon_t \end{array} \right\}^e \end{aligned} \quad (8)$$

where $d\sigma_n$ and $d\tau$ are the increments of normal and shear stresses, $d\varepsilon_n$ and $d\varepsilon_t$ are increment of normal and shear strains, D_{n0} and D_{t0} are model parameters, and p_{atm} represents the atmospheric pressure, taken as 101(kPa).

The increment of plastic strain is given by Eq. 9 based on the theory of plasticity (Chen and Baladi 1985; Dafalias 1986).

$$d\varepsilon^p = \left\{ \begin{array}{c} d\varepsilon_n \\ d\varepsilon_t \end{array} \right\}^p = \langle \Gamma \rangle \mathbf{R} = \frac{\mathbf{n} d\sigma}{K_p} \mathbf{R} \quad (9)$$

where Γ is loading index, a scalar value and the operator $\langle \rangle$ is the Macaulay brackets defining $\langle \Gamma \geq \Gamma \rangle$ if $\Gamma > 0$, and $\langle \Gamma \geq 0 \rangle$ if $\Gamma \leq 0$. The superscript p represents the plastic component.

The loading direction vector (\mathbf{n}) is defined as:

$$\mathbf{n} = \left\{ \begin{array}{c} \partial f / \partial \sigma_n \\ \partial f / \partial \tau \end{array} \right\} \quad (10)$$

where f is the yield surface function, which is used for limiting the elastic deformation. It is a small wedge-type in $\tau-\sigma_n$ space and is expressed as (Dafalias and Manzari 2004; Lashkari 2012):

$$f = \left(\frac{\tau}{\sigma_n} - \alpha \right)^2 - m^2 = (\mu - \alpha)^2 - m^2 = 0 \quad (11)$$

where $\mu = \tau/\sigma_n$ is the stress ratio, α is the back stress ratio, which defines the center of the yield surface (i.e. $\alpha = \mu^{cs}$), and m controls the size of opening of the wedge-type yield surface. Selecting a constant value for m of about $0.01\mu^{cs}$ - $0.05\mu^{cs}$ has proven to yield satisfactory accuracy (Papadimitriou and Bouckovalas 2002; Taiebat and Dafalias 2008; Saberi et al. 2016; Saberi, Annan, and Konrad 2019). μ^{cs} is critical state stress ratio which is a model parameter and the slope of the critical state line in the $\tau-\sigma_n$ space.

A non-associated flow rule (i.e. $\mathbf{R} \neq \mathbf{n}$) was adopted in this constitutive model. The flow direction vector (\mathbf{R}) which represents the direction of plastic strain increment is defined by Eq. 12.

$$\mathbf{R} = \left\{ \begin{array}{c} D \\ \partial f / \partial \tau \end{array} \right\} \quad (12)$$

where D is the dilatancy coefficient and is given by Eq. 13.

$$D = \frac{d\varepsilon_n^p}{|d\varepsilon_t^p|} = A^d (\mu^{cs} \exp(K^d \psi) - s\mu) \quad (13)$$

where A^d and K^d are two positive model parameters, and s is the auxiliary parameter for which $s = +1$ if $\mu - \alpha \geq 0$, and $s = -1$ if $\mu - \alpha < 0$.

Based on laboratory and numerical studies (DeJong and Westgate 2009; Evgin and Fakharian 1996; Liu, Song, and Ling 2006), a granular soil–structure interface under large shear displacement reaches an ultimate state called critical state in soil–structure interface problems, analogous to the concept of critical state in soil mechanics. In Eq. 13, ψ is the state parameter, originally introduced by Been and Jefferies (Been and Jefferies 1985) in the framework of CSSM for sands. In this study, the modified state parameter (ψ) (Liu and Ling 2008; Liu, Song, and Ling 2006) is used, as defined by Eq. 14:

$$\psi = e - e_{cs} \quad (14)$$

where e is the void ratio at the current state and e_{cs} is the critical state void ratio corresponding to the current value of normal stress. For states denser than critical state, $\psi < 0$, whereas for states looser than critical state, $\psi > 0$. On the critical state, $\psi = 0$.

Based on experimental observations (Uesugi, Kishida, and Tsubakihara 1989; Zhang and Zhang 2006, 2009a), granular soil–structure interfaces may experience particle breakage during shear cycles which results in more accumulative contraction. Laboratory tests also show that the amount of particle breakage can be correlated with total input energy or total plastic work of the system (Lade, Yamamuro, and Bopp 1996; Uesugi, Kishida, and Tsubakihara 1989; Zeghal and Edil 2002) and particle breakage translates the critical state line (CSL) downward towards smaller void ratio in the e - $\log p'$ plane (Daouadji, Hicher, and Rahma 2001; Ghafghazi, Shuttle, and DeJong 2014). Thus, in the interface model, for simulating the effect of particle breakage, the CSL is translated towards smaller void ratio in the e - $\ln(\sigma_n/p_{atm})$ plane. For this, e_{cs} in Eq. 14 is defined by reformulating the approach suggested by Liu and Zou (2013) for monotonic behavior of gravelly soils (Eq.15).

$$e_{cs} = e_{0-Br} - \lambda \ln\left(\frac{\sigma_n}{p_{atm}}\right) = e_{0-cs}\left(1 - \frac{w_p}{b_{r1} + b_{r2}w_p}\right) - \lambda \ln\left(\frac{\sigma_n}{p_{atm}}\right) \quad (15)$$

where e_{cs-0} , λ , b_{r1} and b_{r2} are model parameters, $w_p/(b_{r1} + b_{r2}w_p) = B_r$ is breakage index and w_p is the total plastic work which can be calculated using the modified plastic work expression (Hu et al. 2011) given by:

$$w_p = \int (\sigma_n \langle d\varepsilon_n^p \rangle + \tau d\varepsilon_t^p) \quad (16)$$

In Eqs. 7 and 9, K_p is the plastic modulus. Following the concept of the two-surface plasticity theory (Dafalias 1986; Dafalias and Popov 1975), K_p is defined for the interface model used in this study by Eq. 17.

$$K_p = K_{p0} \frac{D_{t0} \sqrt{\sigma_n/p_{atm}}}{|\mu - m|} (\mu^{cs} - s\mu) \quad (17)$$

where K_{p0} is a model parameter. All other parameters have previously been defined.

4. Identification and Calibration of Models' Parameters

4.1. Slab and Plinth

A linear elastic model is used to simulate the behavior of the concrete face slab and plinth. These parts are assumed to have a mass density $\rho = 2400 \text{ kg/m}^3$, elasticity Young's modulus $E = 25 \text{ GPa}$, and Poisson's ratio $\nu = 0.17$.

4.2. Rockfills

The cap plasticity model requires three parameters (mass density ρ , elasticity Young's modulus E and Poisson's ratio ν) for elastic behavior and five more parameters to simulate elastoplastic behavior (cohesion d , friction angle β , transition surface radius α , flow stress ratio K and cap eccentricity R). To obtain d and β , the at-failure stresses in triaxial tests is plotted in the plane of $p-t$. The best fitted straight line is then obtained. The slope of the fitted line and its intersection with the t axis give β and d respectively. α is a small number which is typically between 0.01 and 0.05 and K can have a value between 0.778 and 1 to ensure the convexity of the yield surface in the deviatoric plane. Further details about identification of on how to obtain the model parameters can be found in Helwany (2007). As can be observed in Fig. 1, the CFR dam in the present study consists of four rockfill zones (cushion zone, transition zone, main rockfill zone and sub-rockfill zone). Owing to the large particle size of these rockfill and the absence of triaxial test data, the model parameters for these four zones were estimated using triaxial test data obtained by Marachi, Chan, and bolton (1972) and Marsal (1967) for similarly large rockfill materials. The rockfill material parameters used in this study are provided in Table 1. Figure 3 shows a comparison between results of the numerical simulations of triaxial tests carried out in this study and the experimental data for the rockfill material used in the transition zone of the dam. As can be observed, the numerical simulations using the cap plasticity constitutive model predict well the stress-strain relationships and volumetric behavior of the rockfill material under different confining pressures.

4.3. Concrete Face-cushion Layer Interface

The interface model used for simulating the interface zone between the concrete face and cushion layer requires 10 calibration parameters in total: two for elasticity (D_{t0} and D_{n0}), three for critical state (e_{cs-0} , λ and μ^{cs}), two for dilatancy (A^d and K^d), one for hardening (K_{p0}) and

Table 1. Model parameters for rockfill materials.

Parameters	Zone			
	Cushion	Transition	Main Rockfill	Sub Rockfill
Mass Density, ρ (Kg/m^3)	2000	2000	1980	1980
Young's modulus, E (MPa)	200	200	135	125
Poisson's ratio, ν	0.2	0.2	0.2	0.2
Cohesion, d (MPa)	1×10^{-5}	1×10^{-5}	1×10^{-5}	1×10^{-5}
Friction angle, β (deg)	57	56.5	62	61
Transition surface radius, α	0.01	0.01	0.01	0.01
Flow stress ratio, K	1	1	1	1
Cap eccentricity, R	0.4	0.45	0.1	0.1

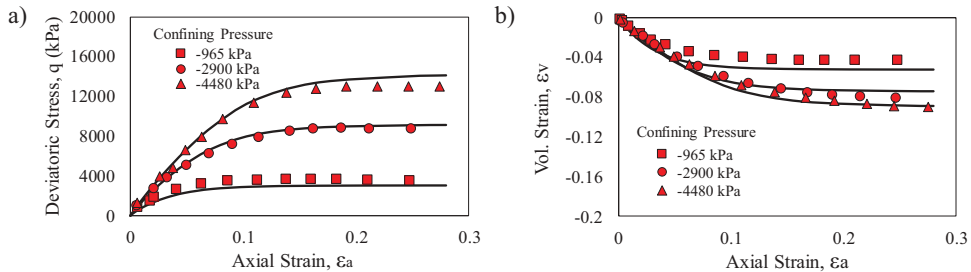


Figure 3. Comparison of model prediction and experimental test for the rockfill material (data from Marachi, Chan, and bolton 1972), a) q - ϵ_a , and b) ϵ_a - ϵ_v .

two for particle breakage (b_{r1} and b_{r2}). The parameters all have physical meaning and can be readily determined through standard interface shear tests: Constant Normal Load (CNL) and Constant Normal Stiffness (CNS) shear test. Details regarding CNL and CNS tests can be found in Evgin and Fakharian (1996), Zhang and Zhang (2006), DeJong and Westgate (2009), and Saberi, Annan, and Konrad (2018a, 2018c).

The D_t and D_n are evaluated as the initial slopes of the shear stress-tangential displacement under CNL condition and normal stress-normal displacement, respectively. With D_t and D_n and using Eq. 8, the elasticity parameters D_{t0} and D_{n0} are obtained. If the shear stresses at critical state (τ_{cr}) are plotted against the corresponding normal stresses (σ_{n-cr}), the slope of the best fitted line starting from the origin is obtained as μ^{cs} . For capturing e_{cs-0} and λ , one can plot the critical void ratios (e_{cr}) at different normal stresses (σ_n) against $\ln(\sigma_n/p_{atm})$. The slope of the best fitted line of the points represents λ and the intersection of the fit line with the e_{cr} axis is given as e_{cs-0} .

The parameter A^d is calculated using the data of monotonic interface shear tests in normal displacement (u_n)-tangential displacement (u_t) plane. $u_n = \epsilon_n \times t_{intf}$ and $u_t = \epsilon_t \times t_{intf}$ in which t_{intf} is the interface thickness. Assuming the elastic parts of normal and tangential displacements are negligible, the following equation can be drawn from Eq. 13.

$$A^d \approx \frac{(du_n/|du_t|)}{\mu^d - \mu} \quad (18)$$

where $\mu^d = \mu^{cs} \exp(K^d \psi)$ is the dilatancy stress ratio.

Using the data obtained from different CNL or CNS tests, the average value of A^d calculated by Eq. 18 is recommended for use in the interface model.

Using the data at phase transformation state, the parameter K^d is calculated from Eq. 19 below.

$$K^d = \frac{\ln\left(\frac{\mu^d}{\mu^{cs}}\right)}{\psi_{phs}} \quad (19)$$

where ψ_{phs} is the state parameter at phase transformation state. K^d can be determined as the slope of the best fitted line passing through the origin by plotting ψ_{phs} against $\ln(\mu^d/\mu^{cs})$ at different CNL and CNS interface shear tests.

The parameter K_{p0} can be easily estimated by a trial and error or by equalizing the normal-constant-load shear test for the interface zone to an uniaxial test for soil. In this case, the following relation for an interface under CNL condition can be drawn:

$$d\epsilon_t = \left(\frac{1}{D_t} + \frac{1}{K_p} \right) d\tau \quad (20)$$

By submitting Eq. 17 into Eq. 20, the parameter K_{p0} can be evaluated as:

$$K_{p0} = \frac{1}{\left(\frac{\mu^{cs}-m}{\mu-m} - 1 \right) \left((D_t \frac{d\epsilon_t}{d\tau}) - 1 \right)} \quad (21)$$

There are two methods to determine b_{r1} and b_{r2} . Firstly, by evaluating the particle breakage index (B_r) and total plastic work (w_p) in different cycles of an interface shear test, the parameters b_{r1} and b_{r2} are obtained by fitting a hyperbolic curve between B_r and W_p . The second method is based on trial and error, such that the model prediction in the plane of normal displacement-tangential displacement matches the corresponding cyclic experimental data.

A typical interface behavior between a concrete slab and gravelly cushion layer in CFRDs was experimentally studied by Zhang and Zhang (2008). In the present study, the parameters of the interface model were calibrated using those laboratory test data. The mechanical properties and the parameters of the interface model are listed in Tables 2 and 3, respectively. The comparison between the experimental data and the interface model simulations for the concrete face-cushion layer interface behavior are presented in Fig. 4 for monotonic and Fig. 5 for cyclic loading. As can be observed, the interface model is well capable of simulating stress-displacement relationships and volumetric behavior of the concrete face-cushion layer interface under both monotonic and cyclic conditions.

5. Finite Element Modeling

5.1. FE Mesh and Construction Procedure

In this study, a general purpose finite element (FE) software ABAQUS (Dassault Systèmes 2013) was used as a numerical tool for simulating the CFR dam. The advanced interface model was implemented in ABAQUS through a user-subroutine in the form of a four-node quadrilateral thin-layer interface element as shown in Fig. 1 with its local axes \bar{x} and \bar{y} . The analyses are two-dimensional. The rockfill, slab and plinth of the dam were simulated by a four-node plane-strain quadrilateral element while the concrete slab-cushion layer interface region was simulated by the newly implemented interface element. A fine mesh sizes were used for the transition zone, the cushion layer and the face slab, and a coarser mesh was used for the rockfill body of the dam in order to reduce the computational costs without losing the numerical accuracy. The finite element mesh of the model consists of 1262 elements (four-node quadrilateral) and 1388 nodes.

Table 2. Mechanical properties of the concrete face-cushion layer interface zone.

Average grain size, D_{50} (mm)	Interface thickness, t_{intf} (mm)	Dry unit weight, γ_d (kN/m ³)
20	100	21.5

Table 3. Model parameters for the concrete slab-cushion layer interface of CFR dam.

Elasticity	Critical state			Dilatancy	Hardening	Particle breakage			
D_{t0} (MPa)	D_{n0} (MPa)	e_{cs-0}	λ	μ^{cs}	A^d	K^d	K_{p0}	b_{r1} (MPa)	b_{r2}
5	6	0.27	0.01	0.88	0.4	6	0.68	6.5	1

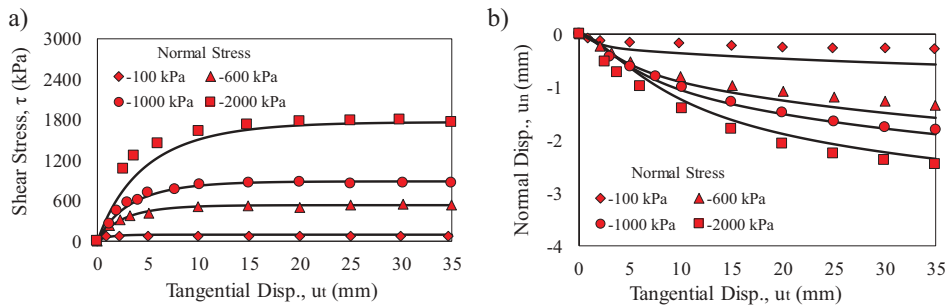


Figure 4. Comparison of interface model prediction and experimental test for the concrete slab-cushion layer interface zone of CFR dam under monotonic constant normal load (CNL) condition (data from Zhang and Zhang 2008), a) $\tau-u_t$, and b) u_n-u_t .

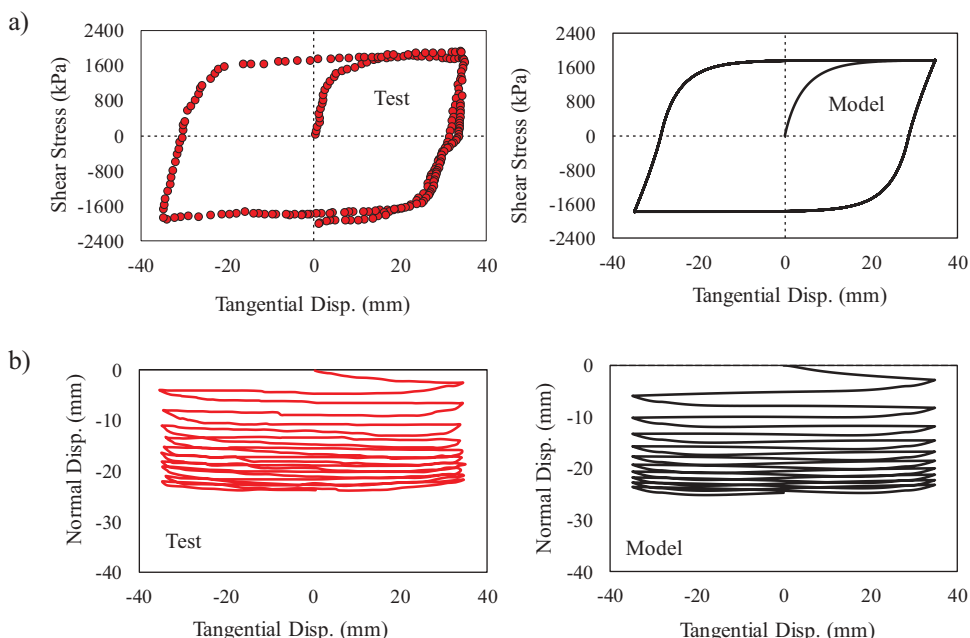


Figure 5. Comparison of interface model prediction and experimental test for the concrete slab-cushion layer interface zone of CFR dam under cyclic constant normal load (CNL) condition with $\sigma_n = -2000$ kPa (data from Zhang and Zhang 2008), a) $\tau-u_t$, and b) u_n-u_t .

The selected dam is located on a rock foundation during the analyses. The finite element model of the dam is presented in Fig. 1.

The construction and impoundment processes were simulated using 40 sub-steps (i.e. 25 stages for dam construction and 15 stages for impoundment). For this, different layers of the material in finite element mesh of the dam are activated sequentially in different sub-steps. The contours of settlements predicted by the numerical model during construction at different stages are illustrated in Fig. 6. The water levels were simulated by the hydrostatic pressures on the concrete face. It should be also mentioned that the compressive and tensile stresses were assumed to be negative and positive, respectively.

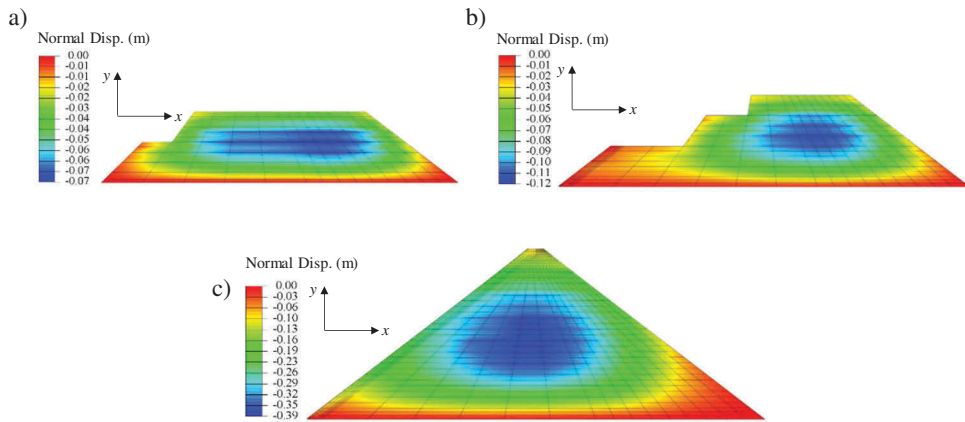


Figure 6. Contours of settlement during construction at different stages in numerical simulation, a) after sub-step 7, b) after sub-step 11, and c) after impoundment.

5.2. Input Ground Motions

As the Toulnustouc dam located in Quebec was selected for this case study, two earthquake ground motion records with magnitude five previously recorded in Rivière-du-Loup, Quebec, Canada were selected for the analyses. These ground motions were recorded in two different stations: NHN with PGA = 0.53 g and station CCN with PGA = 0.41g. PGA is the peak ground acceleration. In order to develop a comparative analysis for the Toulnustouc dam, the selected seismic records were matched with the standard target spectrum of the Quebec region as shown in Fig. 7. The records were selected from the same region with almost similar epicentral distance and magnitude. The acceleration time histories of the earthquake records are illustrated in Fig. 8.

6. Numerical Results and Discussions

6.1. Model Verification

In this section, results of the finite element simulations of the dam during and after impoundment are compared with the field observations. As can be seen from Fig. 9, the numerical model is capable of simulating the crest settlement (Fig. 9a) and horizontal crest

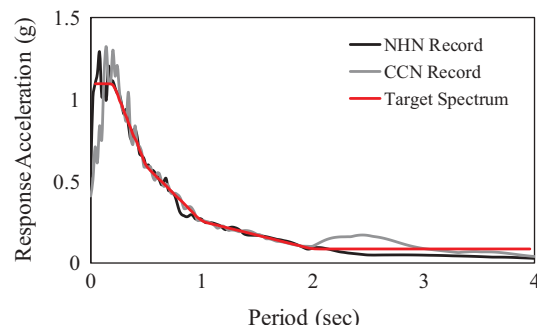


Figure 7. Horizontal acceleration response spectra for the two earthquake records and Quebec target spectrum.

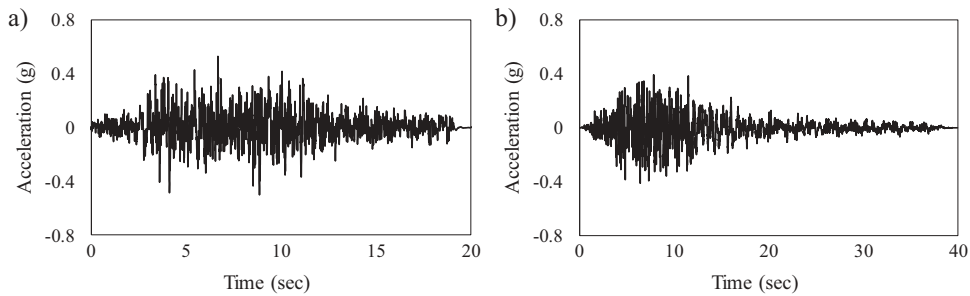


Figure 8. Input ground motion time history, a) NHN station, and b) CCN station.

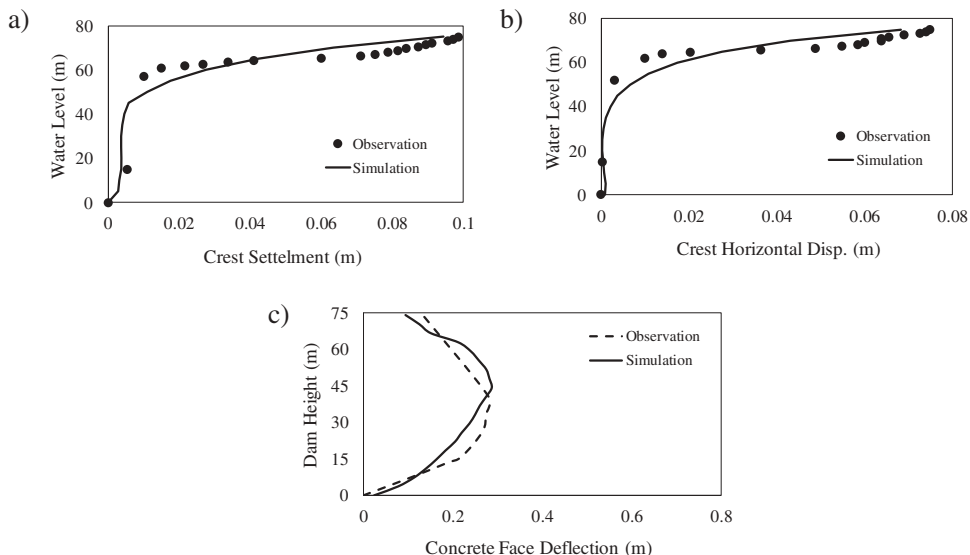


Figure 9. Comparison between the numerical simulations and field, a) crest settlement, b) crest horizontal displacement and c) concrete face deflection.

displacement (Fig. 9b) during impoundment. It also well predicted the concrete slab deflection after impoundment, as illustrated in Fig. 9c.

6.2. Static and Dynamic Responses

In this part, the effect of the seismic ground motions on the performance of the concrete face slab of CFRDs is investigated. The distributions of maximum slab deflection, maximum slope-direction (i.e. parallel to the face slab) stress and maximum horizontal stress of concrete face slab with h/H ratio (i.e. h is vertical distance from the bottom of the dam and H is the dam height) are examined under both static and seismic load conditions. For these analyses, the reservoir water level is assumed to be full (i.e. 75 m) and two different earthquake records described in Sec. 5.2 are used. As can be observed from Fig. 10, the response of the concrete face slab significantly changes under earthquake ground motions over the static condition. The maximum slab deflection increases from about 0.27 m (i.e. 0.36 H%) in the static condition to about

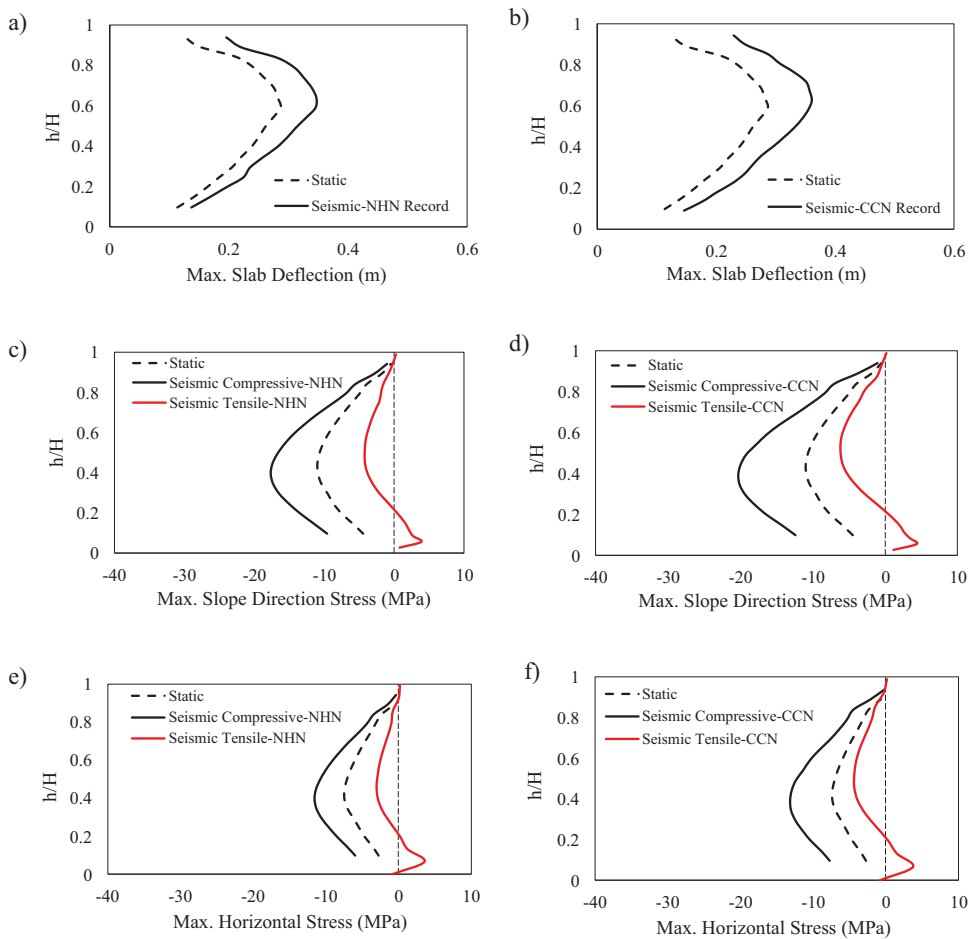


Figure 10. Comparison of static and seismic responses of concrete face slab, a) max. slab deflection under NHHN record, b) max. slab deflection under CCN record, c) max. slope-direction stress under NHHN record, d) max. slope-direction stress under CCN record, e) max horizontal stress under NHHN record, and f) max horizontal stress under CCN record.

0.34 m (i.e. 0.453H%) and 0.37 m (i.e. 0.493H%) under NHHN ([Fig. 10a](#)) and CCN ([Fig. 10b](#)) earthquake records, respectively. It is worth to mention that the slab deflections of 25 in-service CFRDs under static condition were less than 0.4H% based on field observations (Seo et al. 2009; Wen et al. 2017). As can be observed from [Fig. 10c-f](#), the concrete face slab experiences significant compressive and tensile stresses during earthquake. The maximum compressive stress in the slope-direction of the face slab experiences about 50% increase under the NHHN record ([Fig. 10c](#)) and about 75% increase under the CCN record ([Fig. 10d](#)) compared with the static condition. The maximum compressive stress under CCN earthquake loading of about 21 MPa is close to the compressive strength of the concrete slab. Maximum compressive horizontal stress on the concrete face slab increases from 7.35 MPa in the static condition to 11.25 MPa and 13 MPa under NHHN and CCN records, respectively.

The concrete slab experiences significant tensile stresses at the lower parts of the slab, up to about $h/H = 0.2$. If the tensile strength of the concrete is assumed to be 3 MPa

according to Dakoulas (2012b, 2012a), the maximum tensile stresses in concrete face slab in both slope-direction and horizontal direction are larger than the concrete tensile strength under both NHN and CCN records. It shows that concrete face slab may experience serious damages during earthquake ground motions, and this should be considered in the design process of the concrete face slab.

6.3. Water Level

The effect of reservoir water level on the seismic response of concrete face slab in CFR dams is examined in this section. Different reservoir water levels (i.e. 40, 60, and 75 m) are modeled and subjected to the selected earthquake ground motion records. Results of the numerical predictions for the maximum face slab deflections are presented in Fig. 11. As can be observed from Fig. 11, the maximum distribution of face slab deflection under both earthquake ground motions increases significantly by increasing reservoir water level. For instance, under the NHN records, the maximum deflection increases from 0.14 m for reservoir water level of 40 m to about 0.34 m for the full reservoir condition (Fig. 11a). The same behavior can be observed under the CCN record as well. This increase of slab deflection with an increase in the reservoir water level is due to an increase in the applied normal pressure by the water on the face slab.

Figure 12 shows the time histories of the slope-direction and horizontal stresses on the face slab with reservoir water level of 40 m and at full reservoir condition under NHN (Fig. 12a,c) and CCN (Fig. 12b,d) earthquake motion records. These stress-time histories were obtained at a one-third point along the dam height from the foundation. After considering the stress-time histories of a number of points located along the face slab over the height of the dam, it was observed that the concrete face experiences both tensile and compressive stresses during earthquake ground motions. And, the serious compressive and tensile stresses of the concrete face slab under NHN record occurred at about $t = 6.4$ s and $t = 7.0$ s, respectively. The important stress response under CCN ground motion also occurred at around $t = 7.6$ s and $t = 6.9$ s for the compressive and tensile behavior respectively. In order to investigate both maximum compressive and maximum tensile stresses in the face slab under seismic loading condition, the face slab performance at those critical time steps mentioned above are examined. Those critical time steps are highlighted in Fig. 12 for both NHN and CCN records. As can be seen from Fig. 12, the

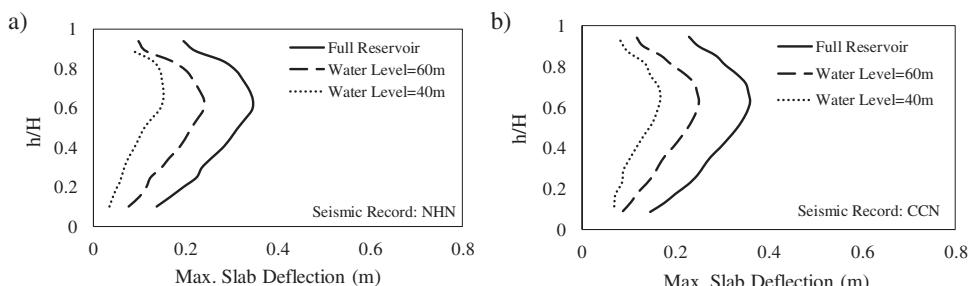


Figure 11. Reservoir water level effect on the maximum deflection of the concrete face slab under, a) NHN record, b) CCN record.

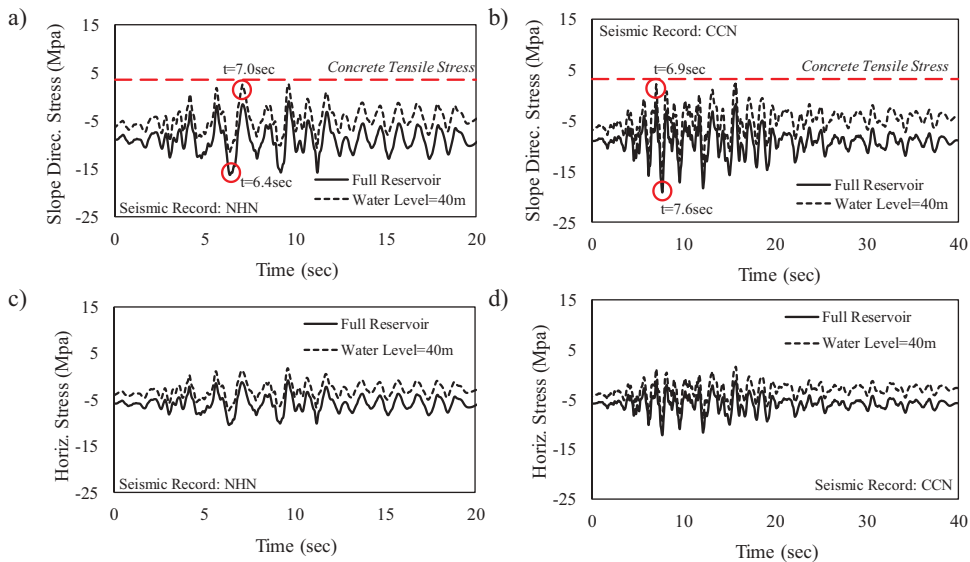


Figure 12. Stress-time history responses of concrete face slab under different reservoir water level, a) slope-direction stress under NHN record, b) slope-direction stress under CCN record, c) horizontal stress under NHN record, and d) horizontal stress under CCN.

face slab experiences serious compressive and tensile stresses. The tensile stress is significantly smaller than the compressive stress and its value increases with a reduction of reservoir water level (Fig. 12). By assuming 3MPa as the tensile strength of the concrete, the concrete face slab experiences tensile stresses close to its tensile strength under both earthquake records as illustrated in Fig. 12.

The face slab stresses in the slope and horizontal directions at $t = 6.4$ s under NHN record and at $t = 7.6$ s under CCN record which are fully compressive also experience considerable increases with rising water level as can be observed in Figs. 13a,c and 14a,c. For example, the maximum compressive stress in the slope-direction of the face slab increases by 47% as the reservoir water level rises from 40 m to its full condition under the NHN earthquake record (Fig. 13a). According to the envelopes of critical stresses in the face slab illustrated in Figs. 13 and 14, it is evident that the location of maximum values in the envelopes of compressive stresses move up along the face slab with increasing reservoir water level. That is, the location of maximum compressive slope-direction and horizontal stresses in face slab increases from around 0.25 h/H for the 40 m reservoir water level to around 0.45 h/H for full reservoir condition. This is due to the upward movement of the reservoir's center of pressure on the face slab by increasing the water level. It is also clear from the envelopes in Figs. 13a,c and 14a,c that by increasing the reservoir water level, the maximum compressive stresses along the face slab experience greater variations.

The envelopes of stresses along the face slab in the slope and horizontal directions at $t = 7.0$ s under NHN record and at $t = 6.9$ s under CCN record are also represented in Figs. 13b,d, and 14b,d to investigate the effect of reservoir water level on the face slab tensile stresses. As can be observed in Figs. 13b,d, and 14b,d, the face slab experiences the tensile stresses mostly at its lower portion except for the case with 40 m reservoir water level in which the envelope of maximum tensile stresses are fully tensile along the face slab. Thus, the compressive stresses in

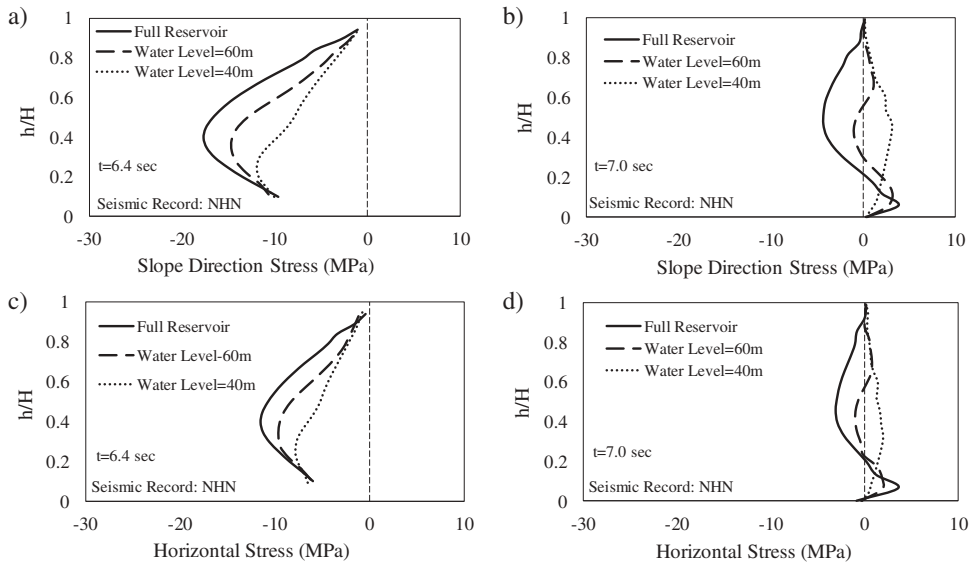


Figure 13. Reservoir water level effect on the stress responses of concrete face slab under NHN record, a) slope-direction stress at $t = 6.4$ s, b) slope-direction stress at $t = 7.0$ s, c) horizontal stress at $t = 6.4$ s, and d) horizontal stress at $t = 7.0$ s.

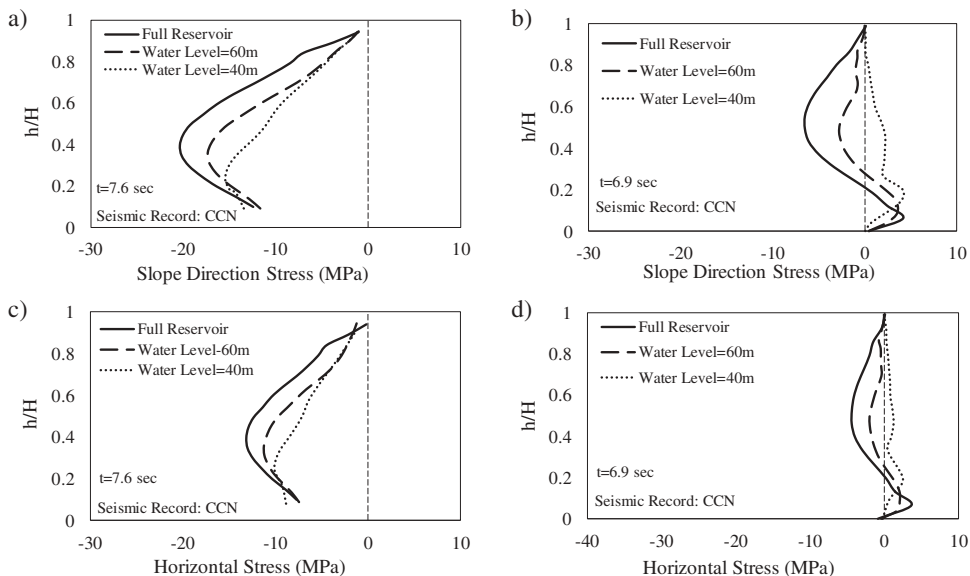


Figure 14. Reservoir water level effect on the stress responses of concrete face slab under CCN record, a) slope-direction stress at $t = 7.6$ s, b) slope-direction stress at $t = 6.9$ s, c) horizontal stress at $t = 7.6$ s, and d) horizontal stress at $t = 6.9$ s.

both slope and horizontal directions decrease, and they are moved towards the tensile stresses. That is, as the reservoir water level decreases, the concrete face slab is more prone to experience tensile stresses along its length under earthquake ground motions. It can be also seen from the

Figs. 13b,d, and 14b,d that the position of maximum tensile values in envelopes of slope-direction and horizontal direction stresses moves up from the lower part of the face slab in full reservoir condition to the middle part of the face slab in 40 m reservoir water level. This is reversed for the position of maximum compressive slope-direction and horizontal stresses, as explained before.

It is worth mentioning that by reducing the reservoir water level, the normal pressure on the upper parts of the face slab is zero while the bottom parts of the face slab experience a non-zero normal pressure, and this pressure is also lower compared with the full reservoir condition. This condition affects the deformation of face slab during earthquake, and it may change the stress distribution along the face slab from being more compressive to more tensile. The interface between the concrete face slab and the cushion layer along the upstream slope also has significant effect of the behavior of the face slab, and it shows different stress-displacement and volumetric behaviors under low to high normal pressures. An interface between a structure and a granular soil under low and high normal pressures experiences very different amount of accumulative contraction under cyclic loading (DeJong and Westgate 2009; Fakharian 1996; Saberi, Annan, and Konrad 2018a), and this results in significant effect on the concrete face slab response during seismic events. The advanced interface element used in this study is capable of simulating the complex stress-displacement relationships and volumetric behavior under various cyclic loading conditions.

Figures 13 and 14 illustrate that slope-direction stresses are larger than horizontal stresses on the face slab under both NHN and CCN earthquake records. The model prediction also shows that the concrete face may experience significant compressive stress (close to -20 MPa) and tensile stresses (more than 3 MPa) along the face slab during earthquake excitations. This shows the extent to which the concrete face slabs in CFR dams are prone to failure under earthquake loading and requires special attention in design.

6.4. Interface Roughness

Interface roughness is an important parameter in soil-structure interface systems which has significant effect on the stress-displacement relationships and volumetric behavior of granular soil-structure interfaces (DeJong and Westgate 2009; Fakharian 1996; Frost, DeJong, and Recalde 2002; Hu and Pu 2004; Koval et al. 2011; Saberi, Annan, and Konrad 2018a; Shahrou and Rezaie 1997; Uesugi, Kishida, and Tsubakihara 1988, 1989). In this section, the numerical simulation of the interface roughness and its effects on the seismic response of concrete face slab is discussed.

6.4.1. Numerical Simulation of Interface Roughness

The interface roughness can be categorized into two general groups of rough and smooth. Based on experimental observations (DeJong and Westgate 2009; Fakharian 1996; Hu and Pu 2004; Shahrou and Rezaie 1997), for smoother structural surfaces, the stress hardening/softening behavior of the interface zones in shear stress (τ)-tangential displacement (u_t) plane gradually becomes negligible and the interface is expected to exhibit an almost elastic-perfectly plastic behavior. Moreover, as the roughness decreases from rough to smooth, the volumetric behavior of the interface changes from contractive/dilative state to a state with negligible volumetric deformation under monotonic condition. Under cyclic loading condition, the stress-displacement behavior for interfaces with different roughness is similar to the monotonic



loading condition (Fakharian 1996; Shahrour and Rezaie 1997). However, by decreasing the interface roughness from rough to smooth, the accumulative contraction is significantly reduced, but still present for smooth surfaces due to cyclic densification of granular soils under cyclic shear loading (Fakharian 1996; Mortara, Ferrara, and Fotia 2010; Mortara, Mangiola, and Ghionna 2007; Shahrour and Rezaie 1997).

The interface constitutive model employed in the FE model of the CFRD is capable of simulating the stress–displacement relationships and volumetric behavior of granular soil–structure interfaces with different roughness. Table 4 shows the model parameters for six interface types with different roughness ranging from rough to smooth. Very rough interface represents the interface type used in the FE model of the case dam (Table 3) presented earlier. The predicted shear stress (τ)-tangential displacement (u_t) and normal displacement (u_n)-tangential displacement (u_t) relationships for the interfaces are shown in Fig. 15 for monotonic loading, and Figs. 16 and 17 for cyclic loading conditions. As can be observed in Figs. 15a and 16, very rough, medium and rough interfaces exhibit stress-hardening characteristics and by reducing roughness, the maximum shear stress is reduced and the behavior shifts towards elastic-perfect plastic in smooth, medium and very smooth interfaces. Furthermore, the volumetric behavior in smooth, medium and very smooth interfaces is negligible as can be observed in Fig. 15b. Under cyclic condition, the interface model predicts the accumulative contraction behavior for the interfaces; however, a reduction in roughness shows less accumulative contractions as represented in Fig. 17.

6.4.2. Effect of Interface Roughness

The effect of interface roughness on the seismic compressive and tensile stress responses of the face slab is examined. Figures 18a,c and 19a,c show the envelopes of stresses in face slab in slope-direction and horizontal direction under NHN record at $t = 6.4$ s and under CCN record at $t = 7.6$ s, which are critical time steps for compressive stresses, with h/H for different interface roughness.

According to the envelopes of maximum compressive stresses along the face slab in slope-direction and horizontal direction (Figs. 18a,c, and Fig. 19a,c), the maximum compressive stresses increases from the lower part of the face slab (i.e. low h/H) up to the middle part around (0.4–0.5) h/H , and then it decreases to the top of the face slab (i.e. $h/H = 1$). This trend remains unchanged by reducing the interface roughness; however, the values of compressive concrete slab stresses decrease. The maximum values in envelopes of compressive slope-direction stresses under both NHN and CCN earthquake records reduced by about 20% by changing the interface roughness from very rough, medium and rough interfaces to very smooth (Figs. 18a and 19a). Similar stress reduction can be observed for the horizontal stresses on the face slab at $t = 6.4$ s for the NHN record and at $t = 7.6$ s for the CCN record (Figs. 18c and 19c). The variation in the envelopes of maximum compressive slope-direction and horizontal stresses

Table 4. Model parameters for different interface roughness.

Interface Type	Parameters									
	D_{t0} (MPa)	D_{n0} (MPa)	e_{cs-0}	λ	μ^{cs}	A^d	K^d	K_{po}	b_{r1} (MPa)	b_{r2}
very rough	5	6	0.27	0.01	0.88	0.4	6	0.68	6.5	1
medium rough	8	9.5	0.27	0.01	0.5	0.3	5	0.68	6.5	1
rough	10	12	0.27	0.01	0.3	0.25	4	0.68	6.5	1
smooth	11	13.5	0.27	0.01	0.2	0.1	1	0.68	6.5	1
medium smooth	12	14.5	0.27	0.01	0.12	0.1	0.3	0.68	6.5	1
very smooth	12	14.5	0.27	0.01	0.1	0.1	0.2	0.68	6.5	1

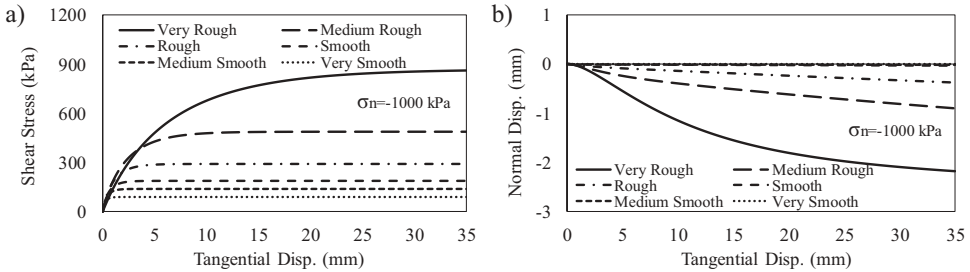


Figure 15. Numerical prediction of granular soil–structure interfaces with different roughness under a constant normal load test (CNL) with the normal stress $\sigma_n = -1000$ kPa, a) shear stress (τ)-tangential displacement (u_t), and b) normal displacement (u_n)-tangential displacement (u_t).

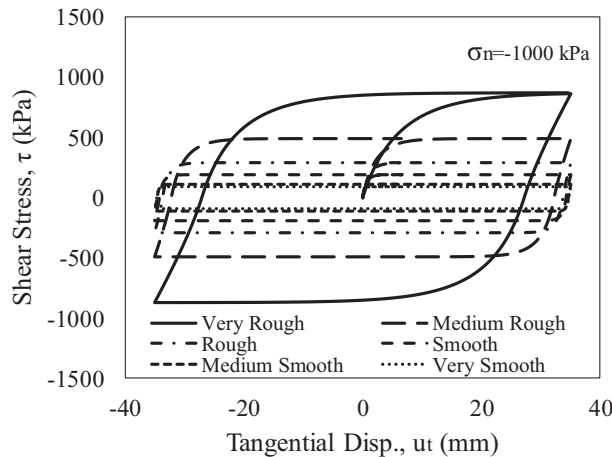


Figure 16. Numerical predictions of shear stress (τ) vs. tangential displacement (u_t) for the interfaces with different roughness using the interface model under a constant normal load test (CNL) with the normal stress $\sigma_n = 1000$ kPa.

by a change in interface roughness is mostly between 0.25 and 0.75 h/H of face slab under both NHN and CCN earthquake records.

Regarding the tensile stress on the face slab, the envelopes of slope-direction and horizontal stresses at critical time steps ($t = 7.0$ s for NHN record and $t = 6.9$ s for CCN record) in which the face slab experiences maximum tensile stresses for different interface roughness are presented in Fig. 18b,d and 19b,d. As can be seen under both NHN (Fig. 18) and CCN (Fig. 19) records, the envelopes of stresses in the slope-direction and the horizontal direction experience tensile condition up to about 0.25 h/H along the face slab for very rough, medium and rough interfaces. However, the tensile zone of the face slab increases up to about 0.4 h/H by reducing the interface roughness to very smooth condition. It can also be observed from the figures that the locations of maximum tensile stresses move up by reducing the interface roughness. That is, the maximum tensile slope-direction stresses under NHN record (Fig. 18b) and CCN record (Fig. 19b) move up from about 0.1 h/H in very rough, medium and rough interfaces to about 0.25 h/H in very smooth interface. The similar behavior is observed for the location of maximum tensile horizontal stresses based on Fig. 18d for NHN record and Fig. 19d for CCN record. However,

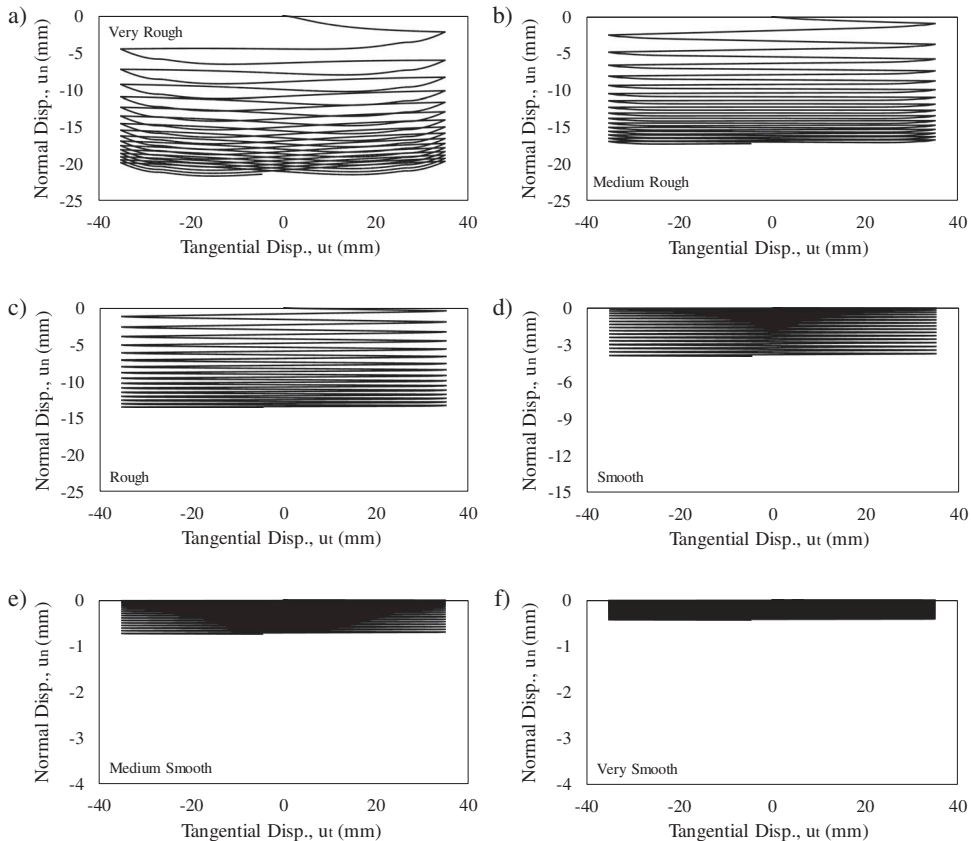


Figure 17. Numerical predictions of tangential displacement (u_t) vs. normal displacement (u_n) for the interfaces with different roughness using the interface model under a constant normal load test (CNL) with the normal stress $\sigma_n = 1000$ kPa.

the location of maximum tensile horizontal stress is around $0.15h/H$ compared to slope-direction stress. According to Fig. 18b,d and Fig. 19b,d, by reducing the interface roughness, both compressive and tensile stresses are reduced significantly. The maximum tensile stresses in slope-direction and horizontal direction experience on average between 40% and 50% reduction from interfaces in the rough category (very rough, medium and rough) to very smooth interfaces under earthquake loading. It is noted that the tensile stresses for medium and very smooth interfaces are below 3MPa, which is assumed as the concrete tensile strength in this study. This considerable reduction of concrete face slab stresses with reduced interface roughness is attributed not only to the stress–displacement relationship within the interface but also to the volumetric behavior of the interface. The volumetric behavior of the granular soil–structure interfaces significantly changes with different interface roughness as explained in section 6.4.1. Accumulative contraction and particle breakage is decreased significantly within the interface zone with reduced roughness and affects the behavior of concrete face slab as the adjacent structure. This is well predicted by the advanced interface model used in this study.

It is noted that the maximum compressive and tensile stress values are almost unchanged for the very rough, medium and rough interface types and they decrease as

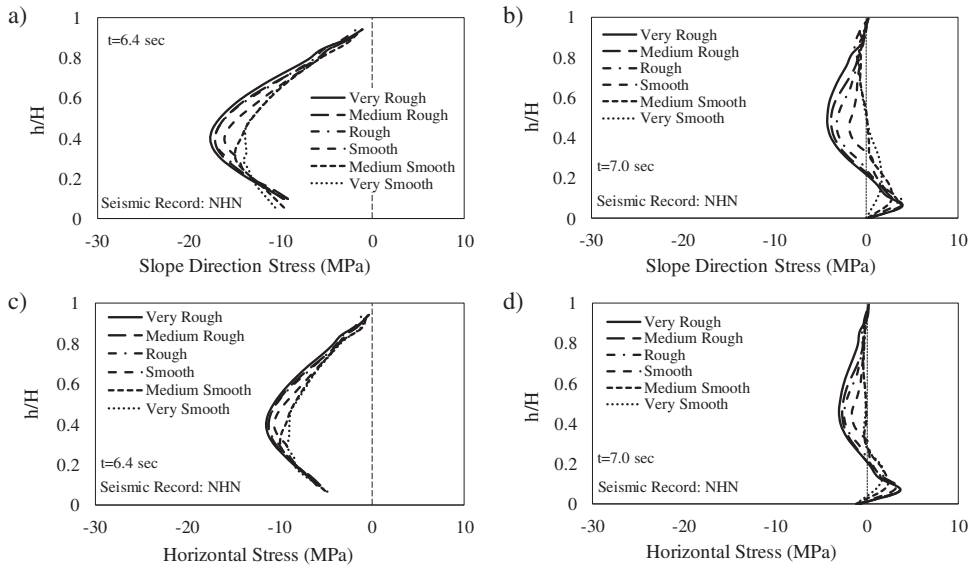


Figure 18. Interface roughness effect on the stress responses of concrete face slab in the CFR dam under NHN record, a) slope-direction stress at $t = 6.4$ s, b) slope-direction stress at $t = 7.0$ s, c) horizontal stress at $t = 6.4$ s, and d) horizontal stress at $t = 7.0$ s.

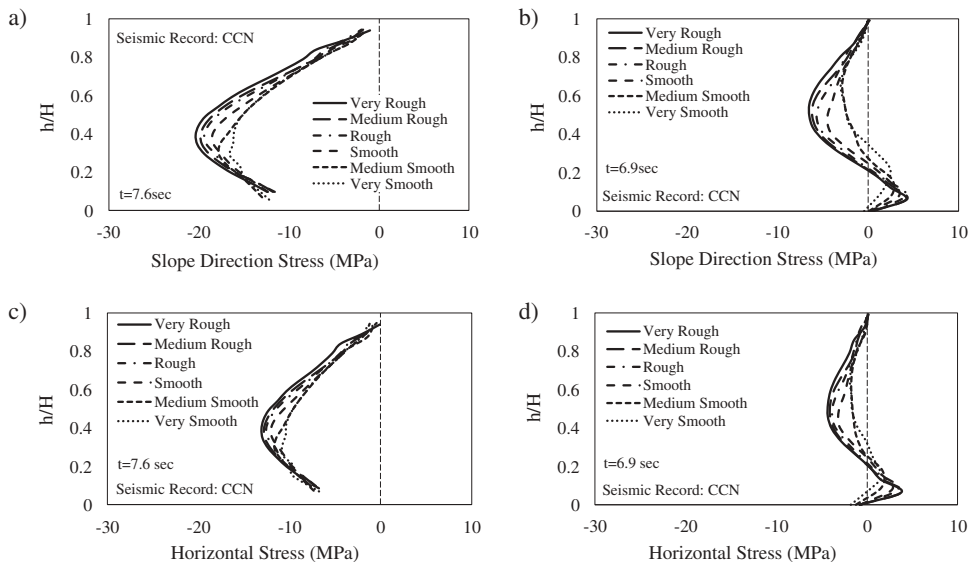


Figure 19. Interface roughness effect on the stress responses of concrete face slab in the CFR dam under CCN record, a) slope-direction stress at $t = 7.6$ s, b) slope-direction stress at $t = 6.9$ s, c) horizontal stress at $t = 7.6$ s, and d) horizontal stress at $t = 6.9$ s.

the interface roughness decreases and becomes smooth, medium and very smooth interfaces (Figs. 18 and 19). From Fig. 20, it appears that there is a near bilinear relationship between the maximum concrete face slab stresses (compressive and tensile) and the roughness at the interface zone. This relationship indicates that there is a certain interface

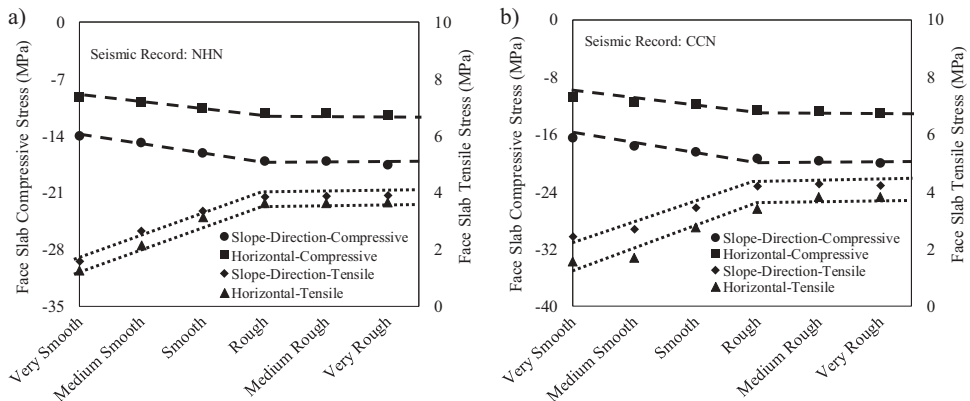


Figure 20. The interface roughness effect on the maximum compressive and tensile stresses of face slab in CFR dams under earthquake excitation, a) NHN seismic record, and b) CCN seismic records.

roughness condition at which a further increase in roughness would not have any significant effect on the maximum stress values. A decrease in interface roughness, however, results in a reduction in both compressive and tensile maximum stresses in the concrete face slab. This observation may provide a useful design information for CFR dams.

6.5. Contact Analysis versus Thin-layer Interface Element

In this section, the seismic response of concrete face slab under earthquake ground motion is investigated using the widely used contact analysis approach and compared with the results from the analysis simulating the face slab-cushion layer interaction using the advanced thin-layer interface element. In the contact analysis, a surface-to-surface contact formulation with Coulomb's friction law was used to represent the interface behavior between the concrete face slab and the cushion layer. This approach neglects the volumetric behavior of interfaces and assumes an elastic-perfectly plastic stress-displacement relationship. The coefficient of friction was chosen as 0.88 in this study, which is equivalent to the critical state stress ratio for the very rough interface. The full reservoir condition of the dam was considered in this analysis for comparison.

The slope-direction and horizontal direction stresses of concrete face slab at critical step times ($t = 6.4$ s and 7.0 s for NHN record and $t = 7.6$ s and 6.9 s for CCN record) versus h/H ratio are illustrated in Fig. 21 for both the contact analysis and thin-layer interface element approaches. As can be observed from Fig. 21, the contact analysis underestimates significantly the stress values in the concrete face slab. Figure 21 shows that contact analysis results in at least 25% reduction in maximum compressive stresses and about 50% reduction in maximum tensile stresses in concrete face slab in the slope-direction and horizontal direction compared to the thin-layer interface element with advance constitutive model. This considerable underestimation by the contact analysis is due to the neglect of volumetric behavior and the particle breakage effect at the interface zone under cyclic loading. These differences diminish for smooth interfaces.

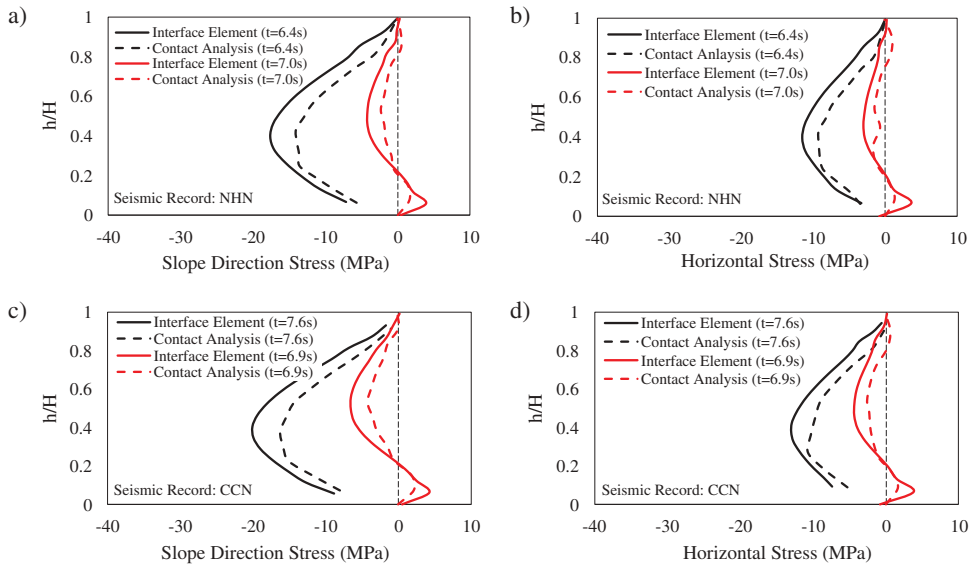


Figure 21. Stress responses of concrete face slab in the CFR dam using contact analysis and thin-layer interface element, a) slope-direction stress under NHN record, b) horizontal stress NHN record, c) slope-direction stress under CCN record, and d) horizontal stress CCN record.

7. Conclusion

This paper has presented a numerical study on the behavior of the concrete face slab in CFRDs by considering the concrete slab-cushion layer interaction under earthquake ground motions. The interface zone was simulated using the thin-layer interface elements defined by an advance constitutive model which was implemented in a finite element code. The interface elements are capable of simulating complex behavior of granular soil-structure interfaces such as stress hardening, critical state, stress degradation, accumulative contraction and particle breakage. The performance of the concrete face slab under static and seismic loading conditions was examined, and the effects of reservoir water level as well as interface roughness on the dynamic response of the concrete face slab were investigated. The effect of interface simulation approach on the seismic response of concrete face slab by comparing the widely used contact analysis and an advanced thin-layer interface element is also examined.

Earthquake ground motions significantly increase the responses of the concrete face slab, such as face slab deflection, slope-direction and horizontal stresses when compared with the static condition. The face slab deflection also increases considerably by an increase in reservoir water level. Regarding the stress behavior of the face slab, an increase in reservoir water level may result in an increase in the maximum compressive stresses (i.e. slope-direction and horizontal). However, by reducing the reservoir water level, the CFR dam may experience tensile stresses along the concrete face slab. The maximum values of stresses in both compressive and tensile within the concrete face slab under earthquake ground motions may cause significant damage in the face slab.

A decrease on the roughness of concrete face-cushion layer interface zone leads to a significant reduction in the concrete face slab compressive and tensile stresses. However,

there is a certain interface roughness beyond which there is no significant increase in maximum stress values in concrete face slab. A reduction on the roughness towards smooth interface results in a reduction in the concrete face slab stress values. Thus, by reducing the friction and volumetric behavior in the face slab-cushion layer interface region in CFR dams, the risk of damage in the face slab under earthquake ground motions is reduced.

The contact analysis approach results in underestimation of both compressive and tensile stresses in the concrete face slab in CFR dams compared to the advanced thin-layer interface element under seismic loading. This is due to the neglect of the volumetric behavior by the contact analysis, which is an important characteristic in soil-structure interface systems.

Acknowledgments

The authors like to acknowledge the financial support of the Natural Sciences and Engineering Research Council of Canada (NSERC). The authors would also like to express their profound gratitude to Mr. Doré Richard from Hydro-Québec for his assistance in providing the field observation data.

References

- Arici, Y. 2011. Investigation of the cracking of CFRD face plates. *Computers and Geotechnics* 38: 905–16. doi:[10.1016/j.compgeo.2011.06.004](https://doi.org/10.1016/j.compgeo.2011.06.004).
- Bayraktar, A., A. A. Dumanoglu, and Y. Calayir. 1996. Asynchronous dynamic analysis of dam-reservoir-foundation systems by the Lagrangian approach. *Computers & Structures* 58: 925–35. doi:[10.1016/0045-7949\(95\)00211-X](https://doi.org/10.1016/0045-7949(95)00211-X).
- Bayraktar, A., K. Hacifendioğlu, and M. Muvaşık. 2005. Asynchronous seismic analysis of concrete-faced rockfill dams including dam-reservoir interaction. *Canadian Journal of Civil Engineering* 32: 940–47. doi:[10.1139/l05-055](https://doi.org/10.1139/l05-055).
- Bayraktar, A., and M. E. Kartal. 2010. Linear and nonlinear response of concrete slab on CFR dam during earthquake. *Soil Dynamics and Earthquake Engineering* 30: 990–1003. doi:[10.1016/j.soildyn.2010.04.010](https://doi.org/10.1016/j.soildyn.2010.04.010).
- Bayraktar, A., M. E. Kartal, and S. Adanur. 2011. The effect of concrete slab-rockfill interface behavior on the earthquake performance of a CFR dam. *International Journal of Non-linear Mechanics* 46: 35–46. doi:[10.1016/j.ijnonlinmec.2010.07.001](https://doi.org/10.1016/j.ijnonlinmec.2010.07.001).
- Been, K., and M. G. Jefferies. 1985. A state parameter for sands. *Géotechnique* 35: 99–112. doi:[10.1680/geot.1985.35.2.99](https://doi.org/10.1680/geot.1985.35.2.99).
- Bouzaïène, H., C. Chartrand, and Y. Hammamji. 2006. Analysis of the behaviour of the Toulnoustouc CFRD dam. Canadian Dam Association (CDA) 2006 Annual Conference, Québec, Quebec city, Canada, 1–8.
- Chen, S., and H. Han. 2009. Impact of the ‘5.12’ Wenchuan earthquake on Zipingpu concrete face rock-fill dam and its analysis. *Geomechanics and Geoengineering* 4: 299–306. doi:[10.1080/17486020903215940](https://doi.org/10.1080/17486020903215940).
- Chen, W. F., and G. Y. Baladi. 1985. *Soil plasticity: Theory and implementation*. New York, NY: Elsevier.
- Chen, Y., R. Hu, W. Lu, D. Li, and C. Zhou. 2011. Modeling coupled processes of non-steady seepage flow and non-linear deformation for a concrete-faced rockfill dam. *Computers & Structures* 89: 1333–51. doi:[10.1016/j.compstruc.2011.03.012](https://doi.org/10.1016/j.compstruc.2011.03.012).
- Clough, G. W., and J. M. Duncan. 1971. Finite element analyses of retaining wall behavior. *Journal of the Soil Mechanics and Foundations Division* 97: 1657–73.
- Cruz, P. T., B. Materón, and M. Freitas. 2010. *Concrete face rockfill dams*. UK: Taylor & Francis.

- Dafalias, Y. F. 1986. Bounding surface plasticity. I: Mathematical foundation and hypoplasticity. *Journal of Engineering Mechanics* 112: 966–87. doi:[10.1061/\(ASCE\)0733-9399\(1986\)112:9\(966\)](https://doi.org/10.1061/(ASCE)0733-9399(1986)112:9(966)).
- Dafalias, Y. F., and E. P. Popov. 1975. A model of nonlinearly hardening materials for complex loading. *Acta Mechanica* 21: 173–92. doi:[10.1007/BF01181053](https://doi.org/10.1007/BF01181053).
- Dafalias, Y. F., and M. T. Manzari. 2004. Simple plasticity sand model accounting for fabric change effects. *Journal of Engineering Mechanics* 130: 622–34. doi:[10.1061/\(ASCE\)0733-9399\(2004\)130:6\(622\)](https://doi.org/10.1061/(ASCE)0733-9399(2004)130:6(622)).
- Dakoulas, P. 2012a. Longitudinal vibrations of tall concrete faced rockfill dams in narrow canyons. *Soil Dynamics and Earthquake Engineering* 41: 44–58. doi:[10.1016/j.soildyn.2012.05.010](https://doi.org/10.1016/j.soildyn.2012.05.010).
- Dakoulas, P. 2012b. nonlinear seismic response of tall concrete-faced rockfill dams in narrow canyons. *Soil Dynamics and Earthquake Engineering* 34: 11–24. doi:[10.1016/j.soildyn.2012.09.007](https://doi.org/10.1016/j.soildyn.2012.09.007).
- Daouadji, A., P.-Y. Hicher, and A. Rahma. 2001. An elastoplastic model for granular materials taking into account grain breakage. *European Journal of Mechanics - A/Solids* 20: 113–37. doi:[10.1016/S0997-7538\(00\)01130-X](https://doi.org/10.1016/S0997-7538(00)01130-X).
- Dassault Systèmes. 2013. *Abaqus documentation*. Providence, RI: Dassault Systèmes Simulia Corp.
- DeJong, J. T., D. J. White, and M. F. Randolph. 2006. Microscale observation and modeling of soil-structure interface behavior using particle image velocimetry. *Soils and Foundations* 46: 15–28. doi:[10.3208/sandf.46.15](https://doi.org/10.3208/sandf.46.15).
- DeJong, J. T., and Z. J. Westgate. 2009. Role of initial state, material properties, and confinement condition on local and global soil-structure interface behavior. *Journal of Geotechnical and Geoenvironmental Engineering* 135: 1646–60. doi:[10.1061/\(ASCE\)1090-0241\(2009\)135:11\(1646\)](https://doi.org/10.1061/(ASCE)1090-0241(2009)135:11(1646)).
- Desai, C. S., J. G. Lightner, and H. J. Siriwardane. 1984. Thin-layer element for interfaces and joints. *International Journal for Numerical and Analytical Methods in Geomechanics* 8: 19–43. doi:[10.1002/nag.1610080103](https://doi.org/10.1002/nag.1610080103).
- DiMaggio, F. L., and I. S. Sandler. 1971. Material model for granular soils. *Journal of the Engineering Mechanics Division* 97: 935–50.
- Drucker, D. C., R. E. Gibson, and D. J. Henkel. 1957. Soil mechanics and work-hardening theories of plasticity. *Transactions of the American Society of Civil Engineers* 122: 338–46.
- Esfahani Kan, M., and H. Taiebat. 2016. Application of an advanced bounding surface plasticity model in static and seismic analyses of Zipingpu Dam. *Canadian Geotechnical Journal* 53: 455–71. doi:[10.1139/cgj-2015-0120](https://doi.org/10.1139/cgj-2015-0120).
- Evgin, E., and K. Fakharian. 1996. Effect of stress paths on the behaviour of sand-steel interfaces. *Canadian Geotechnical Journal* 33: 853–65. doi:[10.1139/t96-116-336](https://doi.org/10.1139/t96-116-336).
- Fakharian, K. 1996. Three-dimensional monotonic and cyclic behaviour of sand-steel interfaces: Testing and modelling. Ph.D. thesis, University fo Ottawa, Ontario, Canada
- Frost, J., J. DeJong, and M. Recalde. 2002. Shear failure behavior of granular–Continuum interfaces. *Engineering Fracture Mechanics* 69: 2029–48. doi:[10.1016/S0013-7944\(02\)00075-9](https://doi.org/10.1016/S0013-7944(02)00075-9).
- Gazetas, G., and P. Dakoulas. 1992. Seismic analysis and design of rockfill dams: State-of-the-art. *Soil Dynamics and Earthquake Engineering* 11: 27–61. doi:[10.1016/0267-7261\(92\)90024-8](https://doi.org/10.1016/0267-7261(92)90024-8).
- Ghaghazi, M., D. A. Shuttle, and J. T. DeJong. 2014. Particle breakage and the critical state of sand. *Soils and Foundations* 54: 451–61. doi:[10.1016/j.sandf.2014.04.016](https://doi.org/10.1016/j.sandf.2014.04.016).
- Helwany, S. 2007. *Applied soil mechanics : With ABAQUS applications*. Hoboken, NJ: John Wiley & Sons.
- Hu, L., and J. Pu. 2004. Testing and modeling of soil-structure interface. *Journal of Geotechnical and Geoenvironmental Engineering* 130: 851–60. doi:[10.1061/\(ASCE\)1090-0241\(2004\)130:8\(851\)](https://doi.org/10.1061/(ASCE)1090-0241(2004)130:8(851)).
- Hu, W., Z. Yin, C. Dano, and P.-Y. Hicher. 2011. A constitutive model for granular materials considering grain breakage. *Science China Technological Sciences* 54: 2188–96. doi:[10.1007/s11431-011-4491-0](https://doi.org/10.1007/s11431-011-4491-0).
- Hydro-Québec. 2006. *Rapport de conception-Aménagement Hydroélectrique de la Toulnustouc*. Montréal, QC: Hydro-Québec.
- Justo, J. L., F. Segovia, and A. Jaramillo. 1995. Three-dimensional joint elements applied to concrete-faced dams. *International Journal for Numerical and Analytical Methods in Geomechanics* 19: 615–36. doi:[10.1002/\(ISSN\)1096-9853](https://doi.org/10.1002/(ISSN)1096-9853).

- Kartal, M. E., A. Bayraktar, and H. B. Bas. 2010. Seismic failure probability of concrete slab on CFR dams with welded and friction contacts by response surface method. *Soil Dynamics and Earthquake Engineering* 30: 1383–99. doi:[10.1016/j.soildyn.2010.06.013](https://doi.org/10.1016/j.soildyn.2010.06.013).
- Kartal, M. E., A. Bayraktar, and H. B. Basaga. 2012. Nonlinear finite element reliability analysis of Concrete-Faced Rockfill (CFR) dams under static effects. *Applied Mathematical Modelling* 36: 5229–48. doi:[10.1016/j.apm.2011.12.004](https://doi.org/10.1016/j.apm.2011.12.004).
- Khalid, B. S., B. Singh, G. C. Nayak, and O. P. Jain. 1990. nonlinear analysis of concrete face rockfill dam. *Journal of Geotechnical Engineering* 116: 822–37. doi:[10.1061/\(ASCE\)0733-9410\(1990\)116:5\(822\)](https://doi.org/10.1061/(ASCE)0733-9410(1990)116:5(822)).
- Khoei, A. R., A. R. Azami, and S. M. Haeri. 2004. Implementation of plasticity based models in dynamic analysis of earth and rockfill dams: A comparison of Pastor-Zienkiewicz and cap models. *Computers and Geotechnics* 31: 384–409. doi:[10.1016/j.compgeo.2004.04.003](https://doi.org/10.1016/j.compgeo.2004.04.003).
- Kong, X., and J. Liu. 2002. Dynamic failure numeric simulations of model concrete-faced rock-fill dam. *Soil Dynamics and Earthquake Engineering* 22: 1131–34. doi:[10.1016/S0267-7261\(02\)00139-2](https://doi.org/10.1016/S0267-7261(02)00139-2).
- Kong, X. J., J. M. Liu, and D. G. Zou. 2016. Numerical simulation of the separation between concrete face slabs and cushion layer of Zipingpu dam during the Wenchuan earthquake. *Science China Technological Sciences* 59: 531–39. doi:[10.1007/s11431-015-5953-6](https://doi.org/10.1007/s11431-015-5953-6).
- Koval, G., F. Chevoir, J. N. Roux, J. Sulem, and A. Corfdir. 2011. Interface roughness effect on slow cyclic annular shear of granular materials. *Granular Matter* 13: 525–40. doi:[10.1007/s10035-011-0267-2](https://doi.org/10.1007/s10035-011-0267-2).
- Lade, P. V., J. A. Yamamuro, and P. A. Bopp. 1996. Significance of particle crushing in granular materials. *Journal of Geotechnical Engineering* 122: 309–16. doi:[10.1061/\(ASCE\)1090-0241\(1997\)123:9\(889\)](https://doi.org/10.1061/(ASCE)1090-0241(1997)123:9(889)).
- Lashkari, A. 2012. A plasticity model for sand-structure interfaces. *Journal of Central South University* 19: 1098–108. doi:[10.1007/s11771-012-1115-1](https://doi.org/10.1007/s11771-012-1115-1).
- Lashkari, A. 2013. Prediction of the shaft resistance of nondisplacement piles in sand. *International Journal for Numerical and Analytical Methods in Geomechanics* 37: 904–31. doi:[10.1002/nag](https://doi.org/10.1002/nag).
- Liu, H., and D. Zou. 2013. Associated generalized plasticity framework for modeling gravelly soils considering particle breakage. *Journal of Engineering Mechanics* 139: 606–15. ©. doi:[10.1061/\(ASCE\)EM.1943-7889.0000513](https://doi.org/10.1061/(ASCE)EM.1943-7889.0000513).
- Liu, H., E. Song, and H. I. Ling. 2006. Constitutive modeling of soil-structure interface through the concept of critical state soil mechanics. *Mechanics Research Communications* 33: 515–31. doi:[10.1016/j.mechrescom.2006.01.002](https://doi.org/10.1016/j.mechrescom.2006.01.002).
- Liu, H., and H. I. Ling. 2008. Constitutive description of interface behavior including cyclic loading and particle breakage within the framework of critical state soil mechanics. *International Journal for Numerical and Analytical Methods in Geomechanics* 32: 1495–514. doi:[10.1002/nag.682](https://doi.org/10.1002/nag.682).
- Liu, J., D. Zou, and X. Kong. 2014. A three-dimensional state-dependent model of soil-structure interface for monotonic and cyclic loadings. *Computers and Geotechnics* 61: 166–77. doi:[10.1016/j.compgeo.2014.05.012](https://doi.org/10.1016/j.compgeo.2014.05.012).
- Loupasakis, C. J., B. G. Christaras, G. C. Dimopoulos, and T. N. Hatzigogos. 2009. Evaluation of plasticity models' ability to analyze typical earth dams' soil materials. *Geotechnical and Geological Engineering* 27: 71–80. doi:[10.1007/s10706-008-9212-5](https://doi.org/10.1007/s10706-008-9212-5).
- Marachi, N. D., C. K. Chan, and S. H. bolton. 1972. Evaluation of properties of rockfill materials. *Journal of the Soil Mechanics and Foundations Division* 98: 95–114.
- Marsal, R. J. 1967. Large-scale testing of rockfill materials. *Journal of the Soil Mechanics and Foundations Division* 93: 27–43.
- Modares, M., and J. E. Quiroz. 2016. Structural analysis framework for concrete-faced rockfill dams. *International Journal of Geomechanics* 16: 1–14. doi:[10.1061/\(ASCE\)GM.1943-5622.0000478](https://doi.org/10.1061/(ASCE)GM.1943-5622.0000478).
- Mortara, G., A. Mangiola, and V. N. Ghionna. 2007. Cyclic shear stress degradation and post-cyclic behaviour from sand–Steel interface direct shear tests. *Canadian Geotechnical Journal* 44: 739–52. doi:[10.1139/t07-019](https://doi.org/10.1139/t07-019).
- Mortara, G., D. Ferrara, and G. Fotia. 2010. Simple model for the cyclic behavior of smooth sand-steel interfaces. *Journal of Geotechnical and Geoenvironmental Engineering* 136: 1004–09. doi:[10.1061/\(ASCE\)GT.1943-5606.0000315](https://doi.org/10.1061/(ASCE)GT.1943-5606.0000315).

- Papadimitriou, A. G., and G. D. Bouckovalas. 2002. Plasticity model for sand under small and large cyclic strains: A multiaxial formulation. *Soil Dynamics and Earthquake Engineering* 22: 191–204. doi:[10.1016/S0267-7261\(02\)00009-X](https://doi.org/10.1016/S0267-7261(02)00009-X).
- Pichler, B., C. Hellmich, H. A. Mang, and J. Eberhardsteiner. 2006. Loading of a gravel-buried steel pipe subjected to rockfall. *Journal of Geotechnical and Geoenvironmental Engineering* 132: 1465–73. doi:[10.1061/\(ASCE\)1090-0241\(2006\)132:11\(1465\)](https://doi.org/10.1061/(ASCE)1090-0241(2006)132:11(1465)).
- Qu, Y., D. Zou, X. Kong, and B. Xu. 2017. A novel interface element with asymmetric nodes and its application on concrete-faced rockfill dam. *Computers and Geotechnics* 85: 103–16. doi:[10.1016/j.compgeo.2016.12.013](https://doi.org/10.1016/j.compgeo.2016.12.013).
- Qu, Y., D. Zou, X. Kong, J. Liu, Y. Zhang, and X. Yu. 2019. Seismic damage performance of the steel fiber reinforced face slab in the concrete-faced rockfill dam. *Soil Dynamics and Earthquake Engineering* 119: 320–30. doi:[10.1016/j.soildyn.2019.01.018](https://doi.org/10.1016/j.soildyn.2019.01.018).
- Saberi, M., C. D. Annan, and J. M. Konrad. 2013. Numerical modeling tools for the analysis of concrete-faced rockfill dams under dynamic earthquake loading. *Proceedings, Annual Conference - Canadian Society for Civil Engineering* 2: 1849–58.
- Saberi, M., C.-D. Annan, and J.-M. Konrad. 2017. Constitutive modeling of gravelly soil-structure interface considering particle breakage. *Journal of Engineering Mechanics* 143 (8): 14. doi:[10.1061/\(ASCE\)EM.1943-7889.0001246](https://doi.org/10.1061/(ASCE)EM.1943-7889.0001246).
- Saberi, M., C.-D. Annan, and J.-M. Konrad. 2018a. On the mechanics and modeling of interfaces between granular soils and structural materials. *Archives of Civil and Mechanical Engineering* 18: 1562–79. doi:[10.1016/j.acme.2018.06.003](https://doi.org/10.1016/j.acme.2018.06.003).
- Saberi, M., C.-D. Annan, and J.-M. Konrad. 2018b. Numerical analysis of concrete faced rockfill dams considering the effect of face slab-cushion layer interaction. *Canadian Geotechnical Journal* 55: 1489–501. doi:[10.1139/cgj-2017-0609](https://doi.org/10.1139/cgj-2017-0609).
- Saberi, M., C.-D. Annan, and J.-M. Konrad. 2018c. A unified constitutive model for simulating stress-path dependency of sandy and gravelly soil-structure interfaces. *International Journal of Non-linear Mechanics* 102: 1–13. doi:[10.1016/j.ijnonlinmec.2018.03.001](https://doi.org/10.1016/j.ijnonlinmec.2018.03.001).
- Saberi, M., C.-D. Annan, and J.-M. Konrad. 2019. Implementation of a soil-structure interface constitutive model for application in geo-structures. *Soil Dynamics and Earthquake Engineering* 116: 714–731. doi:[10.1016/j.soildyn.2018.11.001](https://doi.org/10.1016/j.soildyn.2018.11.001).
- Saberi, M., C.-D. Annan, J.-M. Konrad, and A. Lashkari. 2016. A critical state two-surface plasticity model for gravelly soil-structure interfaces under monotonic and cyclic loading. *Computers and Geotechnics* 80: 71–82. doi:[10.1016/j.compgeo.2016.06.011](https://doi.org/10.1016/j.compgeo.2016.06.011).
- Saberi, M., F. Behnamfar, and M. Vafaeian. 2015. A continuum shell-beam finite element modeling of buried pipes with 90-degree elbow subjected to earthquake excitations. *International Journal of Engineering -transactions C: Aspects* 28: 338–49. doi:[10.5829/idosi.ije.2015.28.03c.02](https://doi.org/10.5829/idosi.ije.2015.28.03c.02).
- Sandler, I. S., and M.L. Baron. 1979. Recent developments in the constitutive modeling of geological materials. In *Proceedings of the 3rd International Conference on Numerical Methods in Geomechanics*, Aachen, Germany, 2–6 April 1979, Balkema, ed. W. Wittke, 363–376. Rotterdam: A.A. Balkema.
- Seiphoori, A., S. M. Haeri, and M. Karimi. 2011. Three-dimensional nonlinear seismic analysis of concrete faced rockfill dams subjected to scattered P, SV, and SH waves considering the dam-Foundation interaction effects. *Soil Dynamics and Earthquake Engineering* 31: 792–804. doi:[10.1016/j.soildyn.2011.01.003](https://doi.org/10.1016/j.soildyn.2011.01.003).
- Seo, M.-W., I. S. Ha, Y.-S. Kim, and S. M. Olson. 2009. Behavior of concrete-faced rockfill dams during initial impoundment. *Journal of Geotechnical and Geoenvironmental Engineering* 135: 1070–81. doi:[10.1061/\(ASCE\)GT.1943-5606.0000021](https://doi.org/10.1061/(ASCE)GT.1943-5606.0000021).
- Shahrour, I., and F. Rezaie. 1997. An elastoplastic constitutive relation for the soil-structure interface under cyclic loading. *Computers and Geotechnics* 21: 21–39. doi:[10.1016/S0266-352X\(97\)00001-3](https://doi.org/10.1016/S0266-352X(97)00001-3).
- Sherard, J. L., and J. Barry Cooke. 1987. Concrete-face rockfill dam: I. Assessment. *Journal of Geotechnical Engineering* 113: 1096–112. doi:[10.1061/\(ASCE\)0733-9410\(1987\)113:10\(1096\)](https://doi.org/10.1061/(ASCE)0733-9410(1987)113:10(1096)).
- Taiebat, M., and Y. F. Dafalias. 2008. SANISAND: Simple anisotropic sand plasticity model. *International Journal for Numerical and Analytical Methods in Geomechanics* 32: 915–48. doi:[10.1002/nag.651](https://doi.org/10.1002/nag.651).

- Uddin, N. 1999. A dynamic analysis procedure for concrete-faced rockfill dams subjected to strong seismic excitation. *Computers & Structures* 72: 409–21. doi:[10.1016/S0045-7949\(99\)00011-5](https://doi.org/10.1016/S0045-7949(99)00011-5).
- Uddin, N., and G. Gazetas. 1995. Dynamic response of concrete-faced rockfill dams to strong seismic excitation. *Journal of Geotechnical Engineering* 121: 185–97. doi:[10.1061/\(ASCE\)0733-9410\(1995\)121:2\(185\)](https://doi.org/10.1061/(ASCE)0733-9410(1995)121:2(185)).
- Uesugi, M., H. Kishida, and Y. Tsubakihara. 1988. Behavior of sand particles in sand-steel friction. *Soils and Foundations* 28: 107–18. doi:[10.3208/sandf1972.28.107](https://doi.org/10.3208/sandf1972.28.107).
- Uesugi, M., H. Kishida, and Y. Tsubakihara. 1989. Friction between sand and steel under repeated loading. *Soils and Foundations* 29: 127–37. doi:[10.3208/sandf.47.887](https://doi.org/10.3208/sandf.47.887).
- Uesugi, M., H. Kishida, and Y. Uchikawa. 1990. Friction between dry sand and concrete under monotonic and repeated loading. *Soils and Foundations* 30: 115–28. doi:[10.3208/sandf1972.30.115](https://doi.org/10.3208/sandf1972.30.115).
- Wen, L., J. Chai, Z. Xu, Y. Qin, and Y. Li. 2017. Monitoring and numerical analysis of behaviour of Miaojiaba concrete-face rockfill dam built on river gravel foundation in China. *Computers and Geotechnics* 85: 230–48. doi:[10.1016/j.compgeo.2016.12.018](https://doi.org/10.1016/j.compgeo.2016.12.018).
- Xianjing, K., Z. Yang, Z. Degao, B. Xu, and L. Yu. 2011. Numerical analysis of dislocations of the face slabs of the Zipingpu concrete faced rockfill dam during the Wenchuan earthquake. *Earthquake Engineering and Engineering Vibration* 10: 581–89. doi:[10.1007/s11803-011-0091-z](https://doi.org/10.1007/s11803-011-0091-z).
- Xu, B., D. Zou, and H. Liu. 2012. Three-dimensional simulation of the construction process of the Zipingpu concrete face rockfill dam based on a generalized plasticity model. *Computers and Geotechnics* 43: 143–54. doi:[10.1016/j.compgeo.2012.03.002](https://doi.org/10.1016/j.compgeo.2012.03.002).
- Xu, B., D. Zou, X. Kong, Y. Zhou, and X. Liu. 2017. Concrete slab dynamic damage analysis of CFRD based on concrete nonuniformity. *International Journal of Geomechanics* 17: 04017055. doi:[10.1061/\(asce\)gm.1943-5622.0000939](https://doi.org/10.1061/(asce)gm.1943-5622.0000939).
- Xu, B., D. Zou, X. Kong, Z. Hu, and Y. Zhou. 2015. Dynamic damage evaluation on the slabs of the concrete faced rockfill dam with the plastic-damage model. *Computers and Geotechnics* 65: 258–65. doi:[10.1016/j.compgeo.2015.01.003](https://doi.org/10.1016/j.compgeo.2015.01.003).
- Zeghal, M., and T. B. Edil. 2002. Soil structure interaction analysis: Modeling the interface. *Canadian Geotechnical Journal* 39: 620–28. doi:[10.1139/t02-016](https://doi.org/10.1139/t02-016).
- Zhang, B., J. G. Wang, and R. Shi. 2004. Time-dependent deformation in high concrete-faced rockfill dam and separation between concrete face slab and cushion layer. *Computers and Geotechnics* 31: 559–73. doi:[10.1016/j.compgeo.2004.07.004](https://doi.org/10.1016/j.compgeo.2004.07.004).
- Zhang, G., and J.-M. Zhang. 2006. Monotonic and cyclic tests of interface between structure and gravelly soil. *Soils and Foundations* 46: 505–18. doi:[10.3208/sandf.46.505](https://doi.org/10.3208/sandf.46.505).
- Zhang, G., and J.-M. Zhang. 2008. Unified modeling of monotonic and cyclic behavior of interface between structure and gravelly soil. *Soils and Foundations* 48: 231–45. doi:[10.3208/sandf.48.231](https://doi.org/10.3208/sandf.48.231).
- Zhang, G., and J.-M. Zhang. 2009a. Constitutive rules of cyclic behavior of interface between structure and gravelly soil. *Mechanics of Materials* 41: 48–59. doi:[10.1016/j.mechmat.2008.08.003](https://doi.org/10.1016/j.mechmat.2008.08.003).
- Zhang, G., and J.-M. Zhang. 2009b. Numerical modeling of soil-Structure interface of a concrete-faced rockfill dam. *Computers and Geotechnics* 36: 762–72. doi:[10.1016/j.compgeo.2009.01.002](https://doi.org/10.1016/j.compgeo.2009.01.002).
- Zhou, M., Z. Bingyin, P. Chong, and W. Wu. 2016b. Three-dimensional numerical analysis of concrete-faced rockfill dam using dual-mortar finite element method with mixed tangential contact constraints. *International Journal for Numerical and Analytical Methods in Geomechanics* 40: 2100–22. doi:[10.1002/nag.2524](https://doi.org/10.1002/nag.2524).
- Zhou, M.-Z., B. Zhang, and Y. Jie. 2016a. Numerical simulation of soft longitudinal joints in concrete-faced rockfill dam. *Soils Found* 56: 379–90. doi:[10.1016/j.sandf.2016.04.005](https://doi.org/10.1016/j.sandf.2016.04.005).
- Zienkiewicz, O. C., B. Best, C. Dullage, and K. G. Stagg (1970) Analysis of nonlinear problems in rock mechanics with particular reference to jointed rock systems. 2nd International Society of Rock Mechanics, Proceedings, Belgrad, 501–09.
- Zou, D., B. Xu, X. Kong, H. Liu, and Y. Zhou. 2013. Numerical simulation of the seismic response of the Zipingpu concrete face rockfill dam during the Wenchuan earthquake based on a generalized plasticity model. *Computers and Geotechnics* 49: 111–22. doi:[10.1016/j.compgeo.2012.10.010](https://doi.org/10.1016/j.compgeo.2012.10.010).